

Helicity controls the direction of fluxes in rotating turbulence

Sébastien Gomé and Anna Frishman

Department of Physics, Technion Israel Institute of Technology, 32000 Haifa, Israel

(Dated: February 24, 2026)

Turbulence sustains out-of-equilibrium energy fluxes shaped by conservation laws. Three-dimensional flows conserve energy and sign-indefinite helicity, both being transferred to small scales. Yet in 3D rotating turbulence, energy is observed to flow simultaneously toward large-scale two-dimensional structures and toward small-scale three-dimensional waves. We uncover the origin of this dual behavior. When sufficiently fast inertial waves interact with a large-scale 2D flow, they conserve their helicity separately by sign, enforcing an inverse transfer of energy from 3D waves to 2D motions and promoting spectral condensation. Slower modes, by contrast, exchange helicity across opposite-sign sectors and thus behave as in non-rotating turbulence, driving a forward transfer from the large-scale 2D flow to small 3D scales. Using a mean-wave kinetic theory, we derive analytical expressions for these competing bi-directional transfers and quantitatively predict the rotation- and Reynolds-number dependence of the large-scale 2D flow in fully nonlinear simulations, unifying the picture from zero to infinite rotation.

Inviscid invariants are expected to control out-of-equilibrium fluxes in turbulent systems. For example, in two dimensions, an inviscid fluid conserves energy and enstrophy (vorticity squared). These two sign-definite scale-related quantities are constrained to flow in opposite directions: energy to large scales and enstrophy to small scales [1, 2]. This leads to self-organization of turbulence into large-scale structures. In contrast, three-dimensional turbulence conserves energy and sign-indefinite helicity (the scalar product between velocity and vorticity) [3]. This leaves the spectral fluxes unconstrained, with a simultaneous transfer of both energy and helicity to small scales [4–6].

Defying this classification, 3D fluids in the presence of external constraints, such as geometry, magnetic field or rotation, can exhibit a dual organization of energy, with simultaneous transfers to large and small scales [7–16]. Rotation, a primary ingredient in geophysical or astrophysical flows, with a crucial role in climate and weather modeling [17, 18], provides a striking example: under rotation, three-dimensional fluctuations take the form of waves and self-organize into large-scale 2D structures [15, 19], although the invariants are identical to those in 3D turbulence.

Meanwhile, when rotation is not too fast, 3D modes can also extract energy from large-scale 2D structures [20, 21], expected from, e.g., spontaneous generation of instabilities [22, 23]. Flows in the Earth’s oceans [24] and atmosphere [25, 26] often lie in this regime. These bi-directional energy pathways in rotating 3D turbulence lack a general understanding: why are large scales energized in the absence of a sign-definite invariant? How can upscale and downscale energy fluxes coexist?

Here we show that, in the presence of rotation, helicity crucially dictates the partition of energy. For moderate rotation rates, after a large-scale 2D flow spontaneously forms, two types of modes exist: fast waves, dominated by rotation, and slow waves, dominated by the 2D shear. For the former, 2D-3D interactions conserve helicity by sign so energy is transferred to the 2D flow, while the lat-

ter break this conservation law and extract energy from the 2D flow. We capture this behavior analytically via a mean-wave kinetic theory, validated with numerical simulations. Our work suggests a general mechanism for the generation of bi-directional fluxes in wave-dominated systems [27, 28].

We consider the 3D Navier-Stokes equations (3DNSE) describing an incompressible fluid in a rotating frame, i.e. subject to a Coriolis force $-2\Omega\mathbf{e}_z \times \mathbf{v}$, in a domain of dimensions (L_x, L_y, L_z) . The flow is forced by a random three-dimensional isotropic forcing \mathbf{f} where $\langle f_{\mathbf{p},i}(t)f_{\mathbf{q},j}(t') \rangle = 2\epsilon(1 - p_i p_j / p^2)\chi_{\mathbf{p}}\delta(\mathbf{p} + \mathbf{q})\delta(t - t')$, $\chi_{\mathbf{p}}$ is restricted to a shell around $k_f = 2\pi/l_f$ and energy is injected at rate ϵ . The Reynolds number, $Re = \epsilon^{1/3}k_f^{-4/3}/\nu$, where ν is the kinematic viscosity, and the Rossby number, $Ro = \epsilon^{1/3}k_f^{2/3}/(2\Omega)$, jointly determine the resulting state. In the following we will also use the combined parameter $Ro_\epsilon = Ro \times \sqrt{Re}$. We use GHOST [29] to solve this system numerically, taking $l_f = L_y/10$ and $L_x = L_z = L_y/2 = \pi$ (and including hyperviscosity).

For low enough Ro , a large-scale 2D mean flow, termed a condensate, spontaneously emerges. This occurs after a transient where an inverse energy cascade among 2D modes develops after they are energized [7]. For our choice of domain geometry, the condensate takes the form of jets, see Fig. 1(a)-(b). We consider the statistical steady state with $\mathbf{U} = \langle \mathbf{v} \rangle = U(y)\mathbf{e}_x$ the jet mean flow. Typically, most of its energy is contained in the lowest mode $k_y = 2\pi/L_y$, so we approximate $U(y) = U'\sqrt{2}/k_y \sin(k_y y)$, where $U' \equiv \sqrt{\int (\partial_y U)^2 (dy/L_y)}$ denotes the rms shear rate. Perhaps the most basic question is: what value does the condensate amplitude U' take as a function of Ro, Re and the box geometry? Here we answer this question in a mixed regime, where not all interactions with the condensate are wave-dominated, thereby completing [30].

The condensate is fueled by 3D waves [30], called inertial waves. For each 3D mode \mathbf{p} ($p_z \neq 0$) there are two wave polarizations $\mathbf{h}_{\mathbf{p}}^s$, such that $i\mathbf{p} \times \mathbf{h}_{\mathbf{p}}^s = s\mathbf{p}h_{\mathbf{p}}^s$, with

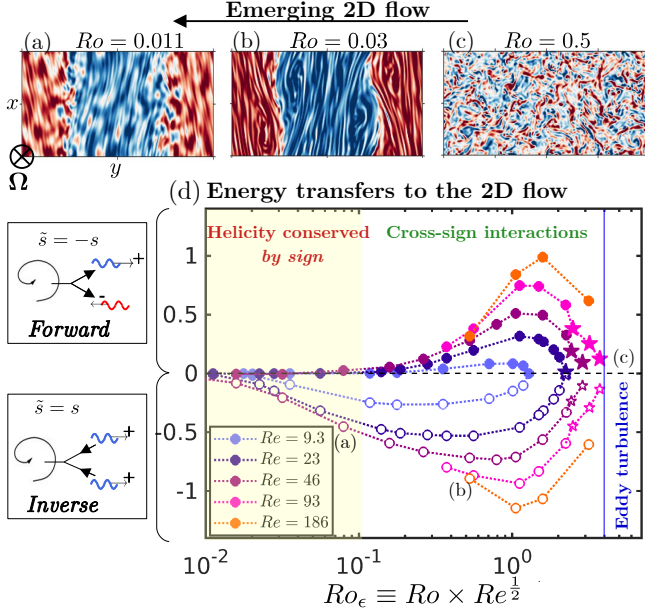


FIG. 1: (a-c) Flow visualizations of vertical vorticity in rotating turbulence. (d) Energy transfers to the 2D condensate in DNS, due to waves of same ($\tilde{s} = s$, hollow circles) or opposite helicity signs ($\tilde{s} = -s$, colored circles), as a function of $Ro_\epsilon \equiv Ro \times Re^{\frac{1}{2}}$. At large rotation, waves conserve their helicity by sign and energize the 2D flow. At low rotation, modes with opposite helicities extract energy from the 2D flow.

chiralities $s = \pm 1$, dispersion relation $\omega_{\mathbf{p}}^s = s2\Omega p_z/p$, and with a given helicity sign $s = \pm 1$. U' is set by the energy transfer between these 3D fluctuations and the condensate, T_{3D-2D} , via the global energy balance:

$$\nu U'^2 = \int \langle uv \rangle \partial_y U \frac{dy}{L_y} = T_{3D-2D} \quad (1)$$

where $\mathbf{u} = \mathbf{v} - U$, $u = \mathbf{u}_x, v = \mathbf{u}_y$, and $\langle uv \rangle$ is the Reynolds stress. Our goal is thus to determine T_{3D-2D} as a function of U' and Ω , allowing to close Eq. (1).

Quasi-Linear Kinetic Theory — As a result of energy condensation, mean-wave interactions dominate over wave-wave interactions ($\mathbf{u} \cdot \nabla \mathbf{u} \ll U \cdot \nabla \mathbf{u}$) for most scales (below a wavenumber denoted by k_U). Fluctuations are therefore governed by quasi-linear (QL) dynamics. Decomposing the fluctuations field into helical waves, $\mathbf{u}(\mathbf{x}) = \sum_{\mathbf{p}, s} a_{\mathbf{p}}^s \mathbf{h}_{\mathbf{p}}^s e^{i\omega_{\mathbf{p}}^s t + i\mathbf{p} \cdot \mathbf{x}}$, we obtain

$$\partial_t a_{\mathbf{p}}^s = \sum_{\substack{\mathbf{q}, \mathbf{k} = \pm \frac{2\pi}{L_y}, \\ \tilde{s} = \pm s}} V_{\mathbf{p}\mathbf{k}\mathbf{q}}^{s\tilde{s}} U_k^* a_{\mathbf{q}}^{\tilde{s}*} e^{-i(\omega_{\mathbf{p}}^s + \omega_{\mathbf{q}}^{\tilde{s}})t} \delta_{\mathbf{k}\mathbf{p}\mathbf{q}} + f_{\mathbf{p}}^s e^{-i\omega_{\mathbf{p}}^s t}, \quad (2)$$

with $\delta_{\mathbf{k}\mathbf{p}\mathbf{q}} = \delta_{\mathbf{k}+\mathbf{p}+\mathbf{q}, 0}$ and $V_{\mathbf{p}\mathbf{k}\mathbf{q}}^{s_1, s_2} = -ip_x (\mathbf{h}_{\mathbf{p}}^{-s_1} \cdot \mathbf{h}_{\mathbf{q}}^{-s_2}) + ik_y (\mathbf{h}_{\mathbf{p}, x}^{-s_1} \mathbf{h}_{\mathbf{q}, y}^{-s_2})$ the coupling coefficients with the 2D mode.

A 3D mode $a_{\mathbf{p}}^s$ interacts with the condensate and with a companion mode $a_{\mathbf{q}}^{\tilde{s}}$ via Eq. 2. The interaction involves

waves of either the same helicity sign $\tilde{s} = s$ (*homochiral-wave interaction*), or of opposite helicity signs $\tilde{s} = -s$ (*heterochiral-wave interaction*). In addition, the helicity exchange between the large-scale 2D flow and the fluctuations is negligible due to scale separation $l_f/L_y \ll 1$, so the helicity of the fluctuations is conserved separately — see [30] and Supplementary Material (SM). Species with opposite helicities can therefore exchange energy (and helicity) only through heterochiral-wave interactions with the condensate.

In classical 3D turbulence, the exchange of energy and helicity between opposite helicity modes [3] results in the transfer of both invariants to smaller scales [4, 6]. As shown in Fig. 1(d), and explained throughout this Letter, introducing rotation progressively suppresses heterochiral-wave interactions, with a profound impact on the energy fluxes. Measuring the energy contribution from waves of either the same helicity sign (hollow circles), or of opposite helicity signs (colored circles), we observe that the condensate is fueled by the former, while the latter extract energy from it.

Rotation acts to select particular interactions, which contribute only if they satisfy the near-resonance condition

$$|\omega_{\mathbf{p}}^s + \omega_{-\mathbf{p}-\mathbf{k}}^{\tilde{s}}| < U', \quad \omega_{\mathbf{p}}^s = s2\Omega \frac{p_z}{p}, \quad (3)$$

for which the frequency sum $\omega_{\mathbf{p}}^s + \omega_{-\mathbf{p}-\mathbf{k}}^{\tilde{s}}$ is sufficiently small so that the interaction does not average-out over the slow time scale $t = o(1/U')$. This can be shown by following wave kinetic theory [30–32], considering the dynamics at the lowest order in time-scale separation U'/Ω [30]. The larger the rotation, the more restrictive condition (3) becomes, decreasing the number of possible interactions.

Condition (3) is more easily satisfied by homochiral-wave interactions ($\tilde{s} = s$), for which it reads $|\omega_{\mathbf{p}}^s + \omega_{-\mathbf{p}-\mathbf{k}}^s| \approx |k_y \partial_p \omega_{\mathbf{p}}^s| < U'$ assuming scale separation $l_f/L_y \ll 1$, than for heterochiral-wave interactions, where it requires $\omega_{\mathbf{p}}^+ + \omega_{-\mathbf{p}-\mathbf{k}}^- \approx 2\omega_{\mathbf{p}}^+ < U'$. Here we work in the regime where homochiral-wave interactions fulfill resonant condition (3), $Ro_\epsilon > l_f/(2L_y)$ (see [30]).

For $\tilde{s} = -s$, a mode \mathbf{p} is involved only in homochiral-wave interactions if it violates the resonance condition (3), and participates in both types of interactions if it satisfies it. Mode \mathbf{p} therefore belongs to one of two sectors:

$$\begin{cases} \text{Sector H: } 2\omega_{\mathbf{p}}^s > U' \text{ (homochiral interactions)} \\ \text{Sector A: } 2\omega_{\mathbf{p}}^s \leq U' \text{ (all interactions),} \end{cases} \quad (4)$$

illustrated in Fig. 2(a). Following (4), modes in sector H have fast frequencies, corresponding to a wave-dominated behavior. In contrast, the dynamics in sector A is shear-dominated and essentially unaffected by rotation. As the frequency $\omega_{\mathbf{p}}^s$ decreases with p , a transition from sector H to sector A occurs when $p > p^* \equiv \frac{4\Omega|p_z|}{U'}$. The rotation

rate, via U'/Ω , therefore controls the number of modes in sectors A and H.

The mean flow $U(y)\mathbf{e}_x$ tends to shear the waves, moving their energy to increasing values of $|p_y|$, while leaving p_x and p_z unchanged. This generates a positive energy flux towards large $|p_y|$, denoted by $\Pi_{\mathbf{p}}^s$ for waves of helicity sign s , whose magnitude at small scales remains to be determined. Energy injected in Sector H thus flows into Sector A ($p > p^*$), see Fig. 2(b). In the following we will compute the energy flux $\Pi_{\mathbf{p}}^s$ in sectors H and A separately. This flux will, in turn, determine the energy transfer to the condensate from modes with given (p_x, p_z, s) , equal to the difference between the energy injected into these modes, ϵ_{p_x, p_z}^s , and the flux to arbitrarily small scales: $\epsilon_{p_x, p_z}^s - \Pi_{|p_y| \rightarrow \infty}^s$.

The spectral energy flux $\Pi_{\mathbf{p}}^s$ is constrained by the conservation of single-sign helicity $H_{\mathbf{p}}^s = sp\langle |a_{\mathbf{p}}^s|^2 \rangle / 2$, occurring in sector H but not in A. This can be seen from the spectral balance for the wave helicity, obtained using scale separation in the QL system:

$$\partial_t H_{\mathbf{p}}^s + \partial_{p_y}(sp\Pi_{\mathbf{p}}^s) = -sp \frac{U'}{\sqrt{2}} \langle uv \rangle_{\mathbf{p}\mathbf{k}}^{s,-s} + sp\epsilon\chi_{\mathbf{p}}^s, \quad (5)$$

where $\Pi_{\mathbf{p}}^s = -U'(\langle a_{\mathbf{p}}^s a_{-\mathbf{p}+\mathbf{k}}^s \rangle + \langle a_{\mathbf{p}}^s a_{-\mathbf{p}-\mathbf{k}}^s \rangle) / (2\sqrt{2})$ and $\langle uv \rangle_{\mathbf{p}\mathbf{k}}^{s,-s} = \Re \left[h_{\mathbf{p},x}^s h_{-\mathbf{p},y}^{-s} (\langle a_{\mathbf{p}}^s a_{-\mathbf{p}+\mathbf{k}}^{-s} \rangle + \langle a_{\mathbf{p}}^s a_{-\mathbf{p}-\mathbf{k}}^{-s} \rangle) \right]$ is the Reynolds stress related to waves of opposite chiralities. The transfer of helicity (and energy) between species s and $-s$ is driven by the opposite-chirality correlators $\langle a_{\mathbf{p}}^s a_{-\mathbf{p}+\mathbf{k}}^{-s} \rangle$ entering $\langle uv \rangle_{\mathbf{p}\mathbf{k}}^{s,-s}$ in Eq. (5).

Energy flux in sector H — In sector H, species s and $-s$ are uncoupled and $\langle uv \rangle_{\mathbf{p}\mathbf{k}}^{s,-s} = 0$. Equation 5 therefore becomes a continuity equation for $H_{\mathbf{p}}^s$: helicity in sector H is conserved *by sign*, which is equivalent to the conservation of wave action $\langle |a_{\mathbf{p}}^s|^2 \rangle / \omega_{\mathbf{p}}^s$ for each species s . Due to this additional sign-definite invariant, the steady-state energy flux solving (5) decays with p_y : $\Pi_{\mathbf{p}}^s = \epsilon_{p_x, p_z}^s k_f / p$ for $p > k_f$. As $\epsilon_{p_x, p_z}^s - \Pi_{|p_y| \rightarrow \infty}^s > 0$, this implies that energy is transferred to the large-scale 2D flow, as depicted in Fig. 2.

At large-enough rotation, all modes are effectively in sector H. In this regime, all waves interacting with the large-scale 2D flow conserve their single-sign helicity: rotation has turned sign-definite an otherwise sign-indefinite invariant. This regime is obtained for $Ro_\epsilon \lesssim 0.1$ in Fig. 1(d), for which the transfer of energy is purely inverse, going *from* the waves *to* the large-scale 2D flow [30, 33]. In contrast, for $Ro_\epsilon \gtrsim 0.1$, heterochiral interactions are possible and generate a finite flux of energy to small scales, as we now explain.

Energy flux in sector A — Modes in sector A are shear-dominated, and their energy balance is typical for a non-rotating flow. There, modes of opposite helicities interact, helicity is no longer conserved by sign, and energy is extracted from the shear flow. Using scale separation $l_f/L_y \ll 1$, the dynamics effectively reduces to that for a linear shear flow, which is analytically solvable when changing variables to fluctuating cross-flow velocity v and

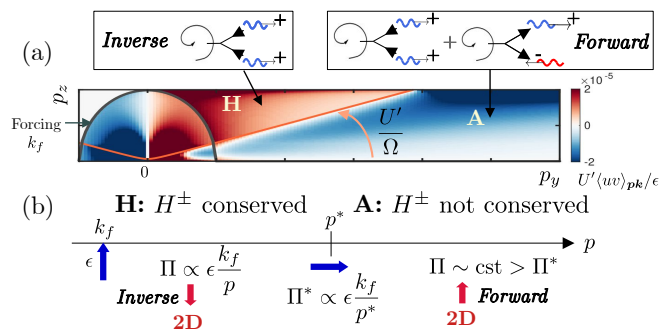


FIG. 2: (a) Energy transfer to the large-scale 2D flow in spectral space (p_y, p_z) from QL theory and (b) schematic of the energy fluxes in the system. Orange line in (a) marks the boundary between Sectors H and A, (4). Waves in sector H conserve their sign-definite helicity $H_{\mathbf{p}}^\pm$, constraining the forward energy flux and causing energy transfer to the 2D flow. In contrast, modes in sector A break this conservation and extract energy from the 2D flow, with resulting energy flux $\Pi > \Pi^*$ (6), Π^* being the energy input from sector H.

vorticity η , see Eq. (12) and [34]. The condensate generates vorticity from z -varying v , which tilts the mean shear (via the RHS of Eq. (12b)), and converts mean-flow energy into turbulent kinetic energy (via Eq. (12c)).

Assuming an incoming flux of $\Pi^*(p_x, p_z)$ at $p = p^*$ into sector A, the flux $\Pi_{\mathbf{p}} \equiv \Pi_{\mathbf{p}}^+ + \Pi_{\mathbf{p}}^-$ can be exactly computed (see End Matter), reading

$$\Pi_{\mathbf{p}} \Big|_{p_y \gg p_y^*} \equiv \frac{\Pi^*}{2} \left[1 + \frac{p^{*2}}{p_0^2} \frac{p_z^2}{p_x^2} \left(\frac{\pi}{2} - \arctan \left(\frac{p_y^*}{p_0} \right) \right)^2 \right], \quad (6)$$

$$\text{with } p^* = \frac{4|p_z|\Omega}{U'}, \quad p_0 = \sqrt{p_x^2 + p_z^2}, \quad p_y^* = (p^{*2} - p_0^2)^{\frac{1}{2}}$$

for large p_y . The small-scale flux is finite (independent of p_y) and can be larger than the incoming energy Π^* , corresponding to an energy extraction from the mean flow. This is most efficient for small p_x (long interaction time with the mean flow) and large p_z (large tilting rate). Note that Sector A can also be directly energized from the forcing shell k_f if $p^* < k_f$, and the resulting energy flux slightly differs (see SM).

Total energy transfer and closure — To combine the results for sector H and A, we take the incoming flux $\Pi^* = \epsilon_{p_x, p_z}(p_x, p_z)k_f/p^*$. The energy transfer to the 2D condensate as a function of the wavenumber \mathbf{p} of inertial waves, $U'\langle uv \rangle_{\mathbf{p}\mathbf{k}}$, can then be computed for a fixed value of U'/Ω (see Eq. (19) and Fig. 2(a)). Waves in sector H transfer energy to the condensate ($U'\langle uv \rangle_{\mathbf{p}\mathbf{k}} > 0$), producing a decaying energy flux, which flows into sector A, where waves extract energy from the condensate ($U'\langle uv \rangle_{\mathbf{p}\mathbf{k}} < 0$), see the schematic Fig. 2(b).

The total energy transfer to the 2D flow, $\epsilon_{p_x, p_z} - \Pi_{|p_y| \rightarrow \infty}$ integrated over (p_x, p_z) , can be found using

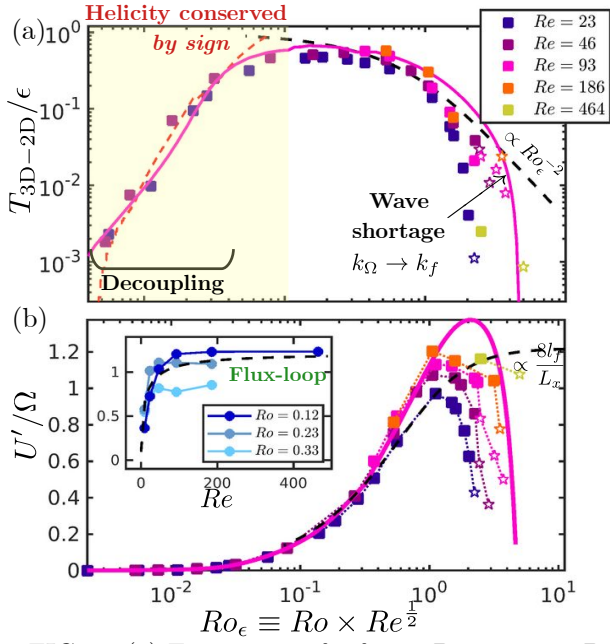


FIG. 3: (a) Energy transfer from 3D waves to 2D condensate and (b) rescaled amplitude of the condensate, as measured from the DNS and predicted from the QL theory. Dashed lines show the predictions in each regime: in black, Eq. (8); in red, the scalings derived in [30]. Solid lines show a numerical solution of the QL system at $Re = 46$, including a wave cutoff k_Ω and a smooth treatment of homochiral-wave near-resonances. Inset in (b): rescaled amplitude of the 2D flow as a function of Re , showing the saturation to a flux-loop state.

Eq. (6), and is equal to

$$\frac{T_{3D-2D}}{\epsilon} \approx \left[1 - \frac{U'}{4\Omega} \left(\frac{19 L_x}{12 \pi l_f} + \frac{1}{2} - \frac{1}{2} \log \frac{U'}{4\Omega} \right) \right] \quad (7)$$

at the leading order in $U'/(4\Omega) \ll 1$, for $U'/\Omega \gtrsim l_f/(2L_y)$ (See SM). From Eq. (7), with increasing U'/Ω (decreasing time-scale separation) the waves transfer less energy to the 2D flow, due to the growth in size of sector A. The dependence of T_{3D-2D} on L_x/l_f in Eq. (7) reflects that the tilting mechanism is most efficient for the largest $p_z/p_x \sim L_x/l_f$.

Finally, to obtain the condensate amplitude, we insert Eq. (7) into the energy balance (1) and obtain

$$\frac{U'}{\Omega} \simeq 2bRo_\epsilon^2 \left(-1 + \sqrt{1 + \frac{1}{b^2 Ro_\epsilon^2}} \right), \quad b = \frac{19 L_x}{48\pi l_f}, \quad (8)$$

at the leading order in L_x/l_f . This solution depends on the single parameter $Ro_\epsilon = Ro \times Re^{1/2}$.

To verify this prediction, we measure the energy transfer from the waves to the 2D flow (Fig. 3(a)), and the amplitude of the 2D flow U'/Ω (Fig. 3(b)) in DNS. Equation

(8) is shown as a dashed line in Fig. 3(b), including sub-leading corrections in $O(1)$ and $O\left(\frac{L_x}{l_f} \sqrt{\frac{l_f}{L_z}}\right)$ — the latter due to discretization errors, non-negligible with our parameter choice (see SM). The corresponding energy transfer, computed from Eq.(1), is shown as a dashed line in Fig. 3(a).

For $Ro_\epsilon \ll 1/b \sim 8l_f/L_x$ (here $\simeq 1.2$ when including subleading corrections), Eq.(8) gives $T_{3D-2D} \simeq \epsilon$ and $U' \simeq \sqrt{\epsilon/\nu}$, corresponding to almost purely homochiral-wave interactions. This is consistent with the DNS behavior in Fig. 1 for $Ro_\epsilon \sim 0.1$. For smaller Ro_ϵ the resonance condition (3) restricts these homochiral-wave interactions, leading to a progressive decoupling between 3D waves and the 2D flow, see the red dashed line in Fig. 3(a) obtained in [30]. The remaining energy is transferred to small-scale waves, which for $Ro_\epsilon \ll l_f/(2L_y)$ is most of the injected energy. Note that the transition from the purely-homochiral to the mixed-interaction regime around $Ro_\epsilon \simeq 0.1$ in the theory (red and black dashed-lines in Fig. 3(a)) is smoothed out when using a smooth function of U'/Ω (21) instead of the sharp near-resonant condition (3) for $\tilde{s} = s$. This perfects the agreement with the DNS in this region (solid line in Fig. 3(a)).

At the other end, for $Ro_\epsilon = Ro \times Re^{1/2} \gg 1/b$, Eq. (8) predicts that $U'/\Omega \rightarrow 1/b$, a Reynolds-independent value. This asymptotic state corresponds to a vanishing energy transfer $T_{3D-2D} \rightarrow 0^+$. For fixed Ro and increasing Re in the DNS, U'/Ω is indeed found to saturate to a constant value, closely following this prediction for the lowest Ro (inset of Fig. 3b), and in accordance with previous observations of rotating turbulence under 3D [35] or 2D forcing [20].

The asymptotic flow state $T_{3D-2D} \xrightarrow{Re \rightarrow \infty} 0^+$ with finite U' is dubbed a *flux-loop state*: a state where inverse and forward energy transfers are almost counterbalanced, see also [8, 10, 12, 20, 21]. This behavior, consistent with taking $\nu \rightarrow 0$ in the energy balance (1), would be impossible if the system strictly conserved two sign-definite quantities, as no steady state would be reached for $Re \rightarrow \infty$. Here, we reveal that the condensate self-tunes to a state of zero large-scale dissipation in this limit, achieved by an exact balance between the inverse energy transfer from modes conserving $H_{\mathbf{p}}^\pm$ (sector H), and the forward transfer due to modes breaking this conservation (sector A). Note that viscosity (and so Re) here primarily affects the *large-scale* dissipation, and could be replaced by, e.g., Ekman friction [36].

From 2D condensates to strong eddy turbulence — When, instead, fixing Re and increasing Ro , the scaling $U' \sim \Omega$ implies a vanishing 2D flow only for zero rotation ($Ro = \infty$), while condensates in DNS disappear to eddy turbulence at $Ro \simeq 0.5$, see Fig. 4. This is due to a shortage of waves at low rotation, and hence of modes in sector H, as we now explain.

When decreasing rotation, more modes behave as eddies instead of inertial waves, i.e. are such that $\tau_{nl}^{\text{eddy}} <$

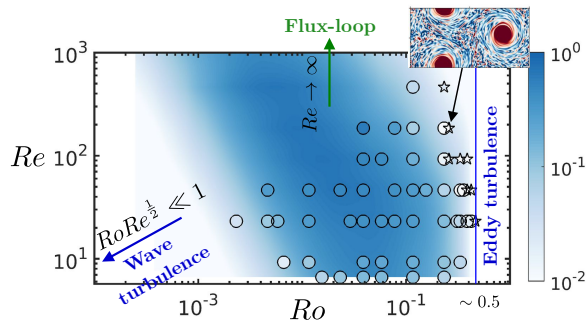


FIG. 4: Heatmap of the energy transfer to the 2D flow, T_{3D-2D} , in the (Ro, Re) plane. The colored background corresponds to the prediction from the QL theory. Stars correspond to a scale-selected vortex lattice.

$\tau_\Omega \equiv 2/\omega_p$ (or, equivalently, $p > k_\Omega \equiv \Omega^{3/5} \epsilon^{-1/5} p_z^{3/5}$ [37]), with $\tau_{nl}^{\text{eddy}} = \epsilon^{-1/3} p^{-2/3}$ the Kolmogorov eddy turnover time. Modes belonging to sector H are such that $\tau_\Omega \lesssim 1/U'$, following Eq. (4). For $p > k_\Omega$, where they behave like eddies and $\tau_{nl}^{\text{eddy}} < \tau_\Omega$, modes do not interact dominantly with the condensate as $\tau_{nl}^{\text{eddy}} < 1/U'$, which breaks the QL approximation. As a consequence, the homochiral sector H, which is the source of energy for the condensate, is cutoff at $p = k_\Omega$ (sector A being cutoff at k_U where eddy-eddy interactions dominate). As rotation is decreased, k_Ω diminishes and the energy input to the condensate is reduced, until no modes exist in sector H when $Ro = 0.5$, for which $k_\Omega(p_z = k_f) = k_f$. This marks the disappearance of condensates to a strong turbulence of 3D eddies. Introducing the wavenumber cutoff into our QL theory and integrating the resulting Reynolds stress numerically, we reproduce the drop in energy transfer and condensate amplitude observed in DNS, see the magenta solid lines in Fig. 3.

Vortex lattice — While jets are found for most Ro and Re , the condensate takes the form of cyclonic vortices at the boundary with 3D turbulence (stars in Figs. 1 and 4), previously observed in [20, 21, 38]. Our theory roughly captures the condensate amplitude for these states, but cannot explain scale selection nor symmetry breaking. The former may be due to time-scale competition between modes of different scales, consistent with the metastability of such states [39].

Conclusion — We have untangled the organization of kinetic energy fluxes in rotating turbulence, showing it is controlled by helicity. Large-scale 2D structures are energized by fast-enough inertial waves via wave-dominated interactions which conserve helicity by sign. In contrast, the 2D flow loses energy to slow waves through shear-dominated interactions which break helicity-by-sign conservation, the waves carrying energy to small scales — similarly to non-rotating 3D turbulence. We have determined these bi-directional energy transfers analytically across rotation regimes via a quasi-linear wave-kinetic theory, which captures the Ro and Re behavior of 2D condensates in Navier-Stokes simulations, as summarized

in Fig. 4.

Our results show that large-scale self-organization can be regulated by a sign-indefinite invariant in the presence of waves [40, 41], and thus arise even in systems that do not conserve multiple sign-definite quantities. The framework developed here provides a route to analyzing such behavior in other settings — such as thin layers [13], chiral flows [12], stratified flows [28, 41–43], magnetohydrodynamics [44, 45], plasmas [46] or geophysical flows [47] — and to elucidating the energy sinks and feedback mechanisms governing their self-organization.

ACKNOWLEDGMENTS

The authors would like to thank the Isaac Newton Institute for Mathematical Sciences, Cambridge, for support and hospitality during the programme “Antidiffusive dynamics: from sub-cellular to astrophysical scales”. This work was supported by BSF grant No. 2022107 and ISF grant No. 486/23.

END MATTER

A. Mean-wave Quasi-Linear Kinetic Theory

We detail here the governing equations and solutions to the quasi-linear system describing the interactions between 3D inertial waves and a large-scale 2D mean flow. We consider a sinusoidal condensate of single mode $\mathbf{k} = \pm 2\pi/L_y$, $U_{\mathbf{k}} = U'/\sqrt{2}\delta_{\mathbf{k}-2\pi/L_y}$. The fluctuation field $\mathbf{u}(\mathbf{x})$ is decomposed into the helical basis $\mathbf{h}_{\mathbf{p}}^s = (\mathbf{p} \times [\mathbf{p} \times \mathbf{e}_z] - ispp \times \mathbf{e}_z)/(\sqrt{2}pp_\perp)$, with $p = |\mathbf{p}|$ and $p_\perp = \sqrt{p_x^2 + p_y^2}$. Following wave kinetic theory, we obtain evolution equations for the wave correlators $\langle a_{\mathbf{p}}^s a_{-\mathbf{p}+\mathbf{k}}^{s'} \rangle$, which we derive from the wave dynamical equation (2) in an expansion in U'/Ω (see [30] and SM §B), and result in the helicity balance (5).

In Sector H, waves conserve their single-sign helicity, via Eq. (5) with $\langle uv \rangle_{\mathbf{p}\mathbf{k}}^{s,-s} = 0$. Introducing the correlator $\Phi_{\mathbf{p}\mathbf{k}}^s \equiv \frac{1}{2}(\langle a_{\mathbf{p}}^s a_{-\mathbf{p}+\mathbf{k}}^{s'} \rangle + \langle a_{\mathbf{p}}^s a_{-\mathbf{p}-\mathbf{k}}^{s'} \rangle)$, Eq. (5) is solved by the energy flux

$$\Pi_{\mathbf{p}}^s \equiv \frac{-U' p_x}{\sqrt{2}} \Phi_{\mathbf{p}\mathbf{k}}^s = \begin{cases} 0 & \text{if } \sigma p_y < -p_y^f \\ \frac{\sigma \epsilon_{p_x, p_z}^s k_f}{2 p} & \text{if } -p_y^f < \sigma p_y < p_y^f \\ \sigma \epsilon_{p_x, p_z}^s \frac{k_f}{p} & \text{if } \sigma p_y > p_y^f, \end{cases} \quad (9)$$

with $\sigma = \text{sgn}(-U' p_x)$, $p_y^f = (k_f^2 - p_x^2 - p_z^2)^{1/2}$ and $\epsilon_{p_x, p_z}^s = \frac{\epsilon}{4\pi \sqrt{k_f^2 - p_x^2 - p_z^2} k_f \nu}$ the energy injected in each line (p_x, p_z) and species s . This flux decaying with p_y , waves lose

energy to the 2D flow via the Reynolds-stress transfer

$$\frac{U'}{\sqrt{2}}\langle uv \rangle_{\mathbf{pk}} = -\frac{U'}{\sqrt{2}} \frac{p_x p_y}{p^3} (\Phi_{\mathbf{pk}}^+ + \Phi_{\mathbf{pk}}^-) \quad (10)$$

which is strictly positive when $\sigma p_y > p_y^f$, and provided that the interaction is resonant at $p = k_f$: $\omega_{\mathbf{p}}^s + \omega_{-\mathbf{p}-\mathbf{k}}^s < U'$.

In Sector A, the 2D flow mediates interactions between modes of opposite helicities, hence correlators $\Psi_{\mathbf{pk}}^s \equiv \frac{1}{2}(\langle a_{\mathbf{p}}^s a_{-\mathbf{p}+\mathbf{k}}^{-s} \rangle + \langle a_{\mathbf{p}}^s a_{-\mathbf{p}-\mathbf{k}}^{-s} \rangle)$ are generated. They are determined from an evolution equation for $\langle a_{\mathbf{p}}^{s*} a_{\mathbf{p}}^{-s} \rangle$:

$$\partial_t \langle a_{\mathbf{p}}^{s*} a_{\mathbf{p}}^{-s} \rangle = \frac{U'}{\sqrt{2}} \left(\mathcal{L}_{\mathbf{p}} [\Psi_{\mathbf{pk}}^{s,-s*} + \Psi_{\mathbf{pk}}^{-s,s}] - 2V_{\mathbf{p}}^{s,-s*} (\Phi_{\mathbf{pk}}^{s*} + \Phi_{\mathbf{pk}}^{-s}) \right), \quad (11)$$

where $\mathcal{L}_{\mathbf{p}} \equiv \left[p_x \partial_{p_y} + \frac{p_x p_y}{p^2} - i \frac{p_z}{p} (1 + 2 \frac{p_x^2}{p^2}) \right]$. Together with Eq. (5), Eq. (11) constitutes a closed system of correlators $(\Phi_{\mathbf{pk}}^s, \Psi_{\mathbf{pk}}^s)$. By changing variables from helical amplitudes $(a_{\mathbf{p}}^+, a_{\mathbf{p}}^-)$ to cross-flow velocity $v_{\mathbf{p}}$ and vorticity $\eta_{\mathbf{p}} \equiv (\nabla \times \mathbf{u})_{\mathbf{p},y}$, we obtain a triangular system of correlators from Eqs. (5)-(11), written in steady state as:

$$\partial_{p_y} \left(p^4 \Re(\langle vv \rangle_{\mathbf{pk}}) \right) = -p^4 \frac{\sqrt{2} \epsilon \chi_{\mathbf{p},y}}{p_x U'} \quad (12a)$$

$$\partial_{p_y} \left(p^2 \langle \eta v \rangle_{\mathbf{pk}} \right) = i p^2 \frac{p_z}{p_x} \langle vv \rangle_{\mathbf{pk}} \quad (12b)$$

$$\partial_{p_y} \Re(\langle \eta \eta \rangle_{\mathbf{pk}}) = \frac{2p_z}{p_x} \Im \langle \eta v \rangle_{\mathbf{pk}} - \frac{\sqrt{2} \epsilon p^2 \chi_{\mathbf{p},y}}{p_x U'}, \quad (12c)$$

with $\langle fg \rangle_{\mathbf{pk}} \equiv (\langle f_{\mathbf{p}} g_{-\mathbf{p}+\mathbf{k}} \rangle + \langle f_{\mathbf{p}} g_{-\mathbf{p}-\mathbf{k}} \rangle)/2$. As the 3D modes have low frequencies in Sector A, rotation has no effect on the leading-order dynamics. Therefore, system (12) describes a non-rotating shear flow interacting with turbulent fluctuations.

Equation (12a) results from the conservation of $\nabla^2 v$ in the mean-turbulent system. Cross-flow velocity v then tilts the mean shear and generates cross-flow vorticity η , via the LHS of (12b). This phenomenon favors modes with large p_z/p_x , whose creation of enstrophy is largest (via Eq. (12c)), hence which dominate the kinetic energy landscape.

For modes with large-enough p_z , such that $p^* = 4|p_z|\Omega/U' > k_f$, and for $U'/\Omega \lesssim 1$, forcing occurs in Sector H and waves there generate a decaying forward energy flux, $\Pi_{\mathbf{k}} \equiv \Pi_{\mathbf{k}}^+ + \Pi_{\mathbf{k}}^- = \sigma(\epsilon_{p_x, p_z}^+(p_x, p_z) + \epsilon_{p_x, p_z}^-(p_x, p_z))k_f/p$, from Eq. (9). This energy flux is transmitted to Sector A at p^* , where it provides a boundary condition for Eqs. (12). Indeed, the energy flux at p^* , $\Pi^* = \sigma(\epsilon_{p_x, p_z}^+(p_x, p_z) + \epsilon_{p_x, p_z}^-(p_x, p_z))k_f/p^*$, determines the values of correlators $\langle vv \rangle_{\mathbf{pk}}(p^*)$, $\langle \eta v \rangle_{\mathbf{pk}}(p^*)$ and $\langle \eta \eta \rangle_{\mathbf{pk}}(p^*)$. Assuming zero helicity injection $\chi_{\mathbf{p}}^s =$

$\chi_{\mathbf{p}}^{-s}$, system (D9) is then solved by:

$$\langle vv \rangle_{\mathbf{pk}} = \frac{\Pi^*}{\sqrt{2}|U'p_x|} \frac{p_0^2 p^{*2}}{p^4} \quad (13)$$

$$\begin{aligned} \langle \eta v \rangle_{\mathbf{pk}} &= i \frac{p_z}{p_x} \frac{1}{p^2} \int_{p_y^*}^{p_y} q^2 \langle vv \rangle_{\mathbf{qk}} dq_y \\ &= i \frac{\Pi^*}{\sqrt{2}|U'p_x|} \frac{p_z}{p_x} \frac{1}{p^2} \left[\arctan\left(\frac{p_y}{p_0}\right) - \arctan\left(\frac{p_y^*}{p_0}\right) \right] \end{aligned} \quad (14)$$

$$\begin{aligned} \langle \eta \eta \rangle_{\mathbf{pk}} &= \frac{p_z}{p_x} \int_{p_y^*}^{p_y} 2\Im \langle \eta v \rangle_{\mathbf{qk}} dq_y + \frac{p_0^2 \Pi^*}{\sqrt{2}|U'p_x|} \\ &= \frac{\Pi^*}{\sqrt{2}|U'p_x|} \frac{p^{*2}}{p^{*2}} \left[\frac{p_0^2}{p^{*2}} + \frac{p_z^2}{p_x^2} \left(\arctan\left(\frac{p_y}{p_0}\right) - \arctan\left(\frac{p_y^*}{p_0}\right) \right)^2 \right] \end{aligned} \quad (16)$$

with $p_0^2 = p_x^2 + p_z^2$ and $p_y^* = (p^{*2} - p_0^2)^{\frac{1}{2}}$. From Eq. (17), we obtain a finite correlator $\langle \eta \eta \rangle_{\mathbf{pk}}$ at large p , responsible for the creation of small-scale cross-flow enstrophy. The small-scale energy flux is then obtained from

$$\begin{aligned} \Pi_{\mathbf{p}} &= -\frac{p_x U'}{\sqrt{2}(p_x^2 + p_z^2)} \left(p^2 \langle vv \rangle_{\mathbf{pk}} + \langle \eta \eta \rangle_{\mathbf{pk}} \right) \\ &= \frac{\sigma \Pi^*}{2} \left[1 + \frac{p^{*2}}{p^2} + \frac{p^{*2}}{p_0^2} \frac{p_z^2}{p_x^2} \left(\arctan\left(\frac{p_y}{p_0}\right) - \arctan\left(\frac{p_y^*}{p_0}\right) \right)^2 \right], \end{aligned} \quad (18)$$

which leads to Eq. (6) when $p \gg p^*$. The energy transfer between the waves and the condensate follows from

$$\begin{aligned} \frac{U'}{\sqrt{2}} \langle uv \rangle_{\mathbf{pk}} &= \sqrt{2} U' \left(-\frac{p_x p_y}{p_x^2 + p_z^2} \langle vv \rangle_{\mathbf{pk}} + \frac{p_z}{p_x^2 + p_z^2} \Im \langle \eta v \rangle_{\mathbf{pk}} \right) \\ &= \begin{cases} k_f \epsilon_{p_x, p_z} \frac{p_y}{2p^3}, & -p_y^f < p_y < p_y^f \quad [\text{Sector H}] \\ k_f \epsilon_{p_x, p_z} \frac{p_y}{p^3}, & p_y^f < p_y < p_y^* \quad [\text{Sector H}] \\ k_f \epsilon_{p_x, p_z} \left[\frac{p^* p_y}{p^4} - \frac{p_z^2}{p_x^2} \frac{1}{p_0} \frac{1}{p^2} \left(\arctan\left(\frac{p_y}{p_0}\right) - \arctan\left(\frac{p_y^*}{p_0}\right) \right) \right], & p_y > p_y^* \quad [\text{Sector A}] \end{cases} \end{aligned} \quad (19)$$

where $\epsilon_{p_x, p_z} = 2\epsilon_{p_x, p_z}^s$ denotes the total energy injected in each line (p_x, p_z) . Figure 1(e) shows this energy transfer, obtained for modes with $p^* > k_f$. A similar approach can be used for slower modes $p^* < k_f$, see SM §E 2, and whose total contribution is found to be negligible. For $p > k_f$, the energy transfer $\frac{U'}{\sqrt{2}} \langle uv \rangle_{\mathbf{pk}}$ is positive in Sector H and negative in Sector A, where waves extract energy from the 2D flow.

Having now determined the Reynolds stress as a function of U'/Ω , we can solve the mean-wave system by

closing with the mean-flow energy balance (1), here non-dimensionalized:

$$\frac{1}{4Ro_\epsilon^2} \left(\frac{U'}{\Omega} \right)^2 = \frac{T_{3D-2D}}{\epsilon} \left[\frac{U'}{\Omega} \right] = \frac{\mathcal{V}}{\sqrt{2}} \int_{s=\pm 1} d\mathbf{p} U' \langle uv \rangle_{\mathbf{p}\mathbf{k}} \quad (20)$$

B. Cutoff and smooth filter

The theory in §A can be refined by including two effects. (i) The QL theory is restricted to modes dominated by the interaction with the condensate. Therefore, the Reynolds stress (19) needs to be cutoff at a wavenumber k_U to exclude wave-wave or eddy-eddy interactions, which start dominating for $p > k_U$. See details in SM §F. Furthermore, Sector H needs to be cutoff at k_Ω , as only wave-like modes ($p < k_\Omega$) are concerned by the selection of homochiral interactions via resonances. The cutoff at k_Ω reduces the energy input to the condensate at high Ro , and causes its decay at $Ro \simeq 0.5$, as $k_\Omega \rightarrow k_f$.

(ii) When $\tilde{s} = s$, the resonance condition (3) can be smoothed to better capture interactions when $\omega_{\mathbf{p}}^s + \omega_{\mathbf{q}}^s \sim U'$, whose contribution is never fully zero nor one. This can be achieved by multiplying the Reynolds stress in (19) by a smooth Lorentzian filter [30, 48],

$$F_{k_f} = \left(1 + \left(\frac{\Omega}{U'} \frac{4\pi p_z \sqrt{k_f^2 - p_x^2 - p_z^2}}{L_y k_f^3} \right)^2 \right)^{-1} \quad (21)$$

In a similar vein, one can refine the resonant condition (3) when $\tilde{s} = -s$ by introducing a parameter $\tilde{\omega}$ in the resonant condition $\omega_{\mathbf{p}}^+ + \omega_{\mathbf{q}}^- < \tilde{\omega} U'$. This is equivalent to changing $\frac{U'}{\Omega} \rightarrow \tilde{\omega} \frac{U'}{\Omega}$ in the theory. Both refinements of (3) can be required to correct our approximate treatment of near-resonances (see [30] and SM §B).

In Fig. 3, solid lines show a numerical solution of the QL system. To produce it, we first integrate numerically the Reynolds stress (given by Eq. (19) for large $p^* > k_f$, but written more generally in SM Eq. (E36)) over a discrete set of wavenumbers $p_z = 2\pi m_z / L_z$ and $p_x = 2\pi m_x / L_x$, ($m_z, m_x \in \mathbb{Z}^*$). We then determine the condensate amplitude U'/Ω and the resulting transfer T_{3D-2D} by solving Eq. 20 in variable U'/Ω via a root-finding procedure. In this integration, $\tilde{\omega}$ is a tuning parameter. In Fig. 3, we use $\tilde{\omega} = 1$. Note that a better agreement with the DNS can be achieved when taking $\tilde{\omega} = 1.2$ (See SM §F 2).

Using the smooth filter (21) results in a smooth transition between the homochiral and the heterochiral interaction regimes around $Ro_\epsilon \simeq 0.1$. Note, however, that this smooth filter is not relevant in the $Ro \rightarrow 0$ limit [30]. Finally, while capturing the disappearance of condensates as $Ro \rightarrow 0.5$, the introduction of cutoff k_Ω causes overshoots before the decay in condensate amplitude. We discuss this effect and its impact on the Re -dependence of the QL solution in SM §F 2.

-
- [1] R. Fjørtoft, *Tellus* **5**, 225 (1953).
 - [2] R. H. Kraichnan, *The Physics of Fluids* **10**, 1417 (1967).
 - [3] R. H. Kraichnan, *Journal of Fluid Mechanics* **59**, 745 (1973).
 - [4] Q. Chen, S. Chen, and G. L. Eyink, *Physics of Fluids* **15**, 361 (2003).
 - [5] P. D. Ditlevsen and P. Giuliani, *Phys. Rev. E* **63**, 036304 (2001).
 - [6] A. Alexakis, *Journal of Fluid Mechanics* **812**, 752 (2017).
 - [7] A. Alexakis and L. Biferale, *Physics Reports* **767**, 1 (2018).
 - [8] G. Boffetta, F. De Lillo, A. Mazzino, and S. Musacchio, *Europhysics Letters* **95**, 34001 (2011).
 - [9] L. M. Smith and F. Waleffe, *Physics of fluids* **11**, 1608 (1999).
 - [10] G. Falkovich and A. G. Kritsuk, *Physical Review Fluids* **2**, 092603 (2017).
 - [11] A. M. Rubio, K. Julien, E. Knobloch, and J. B. Weiss, *Physical Review Letters* **112**, 144501 (2014).
 - [12] X. M. de Wit, M. Fruchart, T. Khain, F. Toschi, and V. Vitelli, *Nature* **627**, 515 (2024).
 - [13] S. J. Benavides and A. Alexakis, *Journal of Fluid Mechanics* **822**, 364 (2017).
 - [14] A. van Kan and A. Alexakis, *Journal of Fluid Mechanics* **864**, 490 (2019).
 - [15] O. Shaltiel, A. Salhov, O. Gat, and E. Sharon, *Physical Review Letters* **132**, 224001 (2024).
 - [16] M. Shavit, O. Bühler, and J. Shatah, *Physical Review Letters* **134**, 054101 (2025).
 - [17] G. K. Vallis and M. E. Maltrud, *Journal of physical oceanography* **23**, 1346 (1993).
 - [18] M. Ghil and V. Lucarini, *Rev. Mod. Phys.* **92**, 035002 (2020).
 - [19] F. S. Godeferd and F. Moisy, *Applied Mechanics Reviews* **67**, 030802 (2015).
 - [20] K. Seshasayanan and A. Alexakis, *Journal of Fluid Mechanics* **841**, 434 (2018).
 - [21] P. Clark Di Leoni, A. Alexakis, L. Biferale, and M. Buzzicotti, *Physical Review Fluids* **5**, 104603 (2020).
 - [22] D. Sipp and L. Jacquin, *Physics of Fluids* **12**, 1740 (2000).
 - [23] P. Billant, *Journal of Fluid Mechanics* **920**, R1 (2021).
 - [24] D. Balwada, J.-H. Xie, R. Marino, and F. Feraco, *Science Advances* **8**, eabq2566 (2022).
 - [25] E. Lindborg, *Geophysical research letters* **32** (2005).
 - [26] A. Czaja, C. Frankignoul, S. Minobe, and B. Vannièrè, *Current climate change reports* **5**, 390 (2019).
 - [27] A. Alexakis, R. Marino, P. D. Mininni, A. van Kan, R. Foldes, and F. Feraco, *Science* **383**, 1005 (2024).
 - [28] V. Labarre and M. Shavit, arXiv preprint

- arXiv:2412.20534 (2024).
- [29] P. D. Mininni, D. Rosenberg, R. Reddy, and A. Pouquet, *Parallel computing* **37**, 316 (2011).
- [30] S. Gomé and A. Frishman, arXiv preprint arXiv:2509.18323 (2025).
- [31] V. E. Zakharov, V. S. L'vov, and G. Falkovich, *Kolmogorov spectra of turbulence I: Wave turbulence* (Springer Science & Business Media, 2012).
- [32] S. Nazarenko, *Wave turbulence*, Vol. 825 (Springer, 2011).
- [33] I. Kolokolov, L. Ogorodnikov, and S. Vergeles, *Physical Review Fluids* **5**, 034604 (2020).
- [34] B. F. Farrell and P. J. Ioannou, *Physics of Fluids A: Fluid Dynamics* **5**, 1390 (1993).
- [35] A. Alexakis, *Journal of Fluid Mechanics* **769**, 46 (2015).
- [36] T. Le Reun, B. Favier, A. J. Barker, and M. Le Bars, *Physical Review Letters* **119**, 034502 (2017).
- [37] O. Zeman, *Physics of Fluids* **6**, 3221 (1994).
- [38] G. Marchetti and P. D. Mininni, arXiv preprint arXiv:2504.05637 (2025).
- [39] J. A. Estrada, A. Alexakis, M. E. Brachet, and P. D. Mininni, arXiv preprint arXiv:2510.06374 (2025).
- [40] L. Biferale, S. Musacchio, and F. Toschi, *Physical Review Letters* **108**, 164501 (2012).
- [41] M. Shavit, O. Bühler, and J. Shatah, *Physical Review Letters* **133**, 014001 (2024).
- [42] G. P. Chini, G. Michel, K. Julien, C. B. Rocha, and C.-c. P. Caulfield, *Journal of Fluid Mechanics* **933**, A22 (2022).
- [43] K. Shah, G. P. Chini, P. C. Colm-cille, and P. Garaud, *Journal of Fluid Mechanics* **998**, A60 (2024).
- [44] A. Pouquet, D. Rosenberg, J. E. Stawarz, and R. Marino, *Earth and Space Science* **6**, 351 (2019).
- [45] B. Gallet, J. Herault, C. Laroche, F. Pétrélis, and S. Fauve, *Geophysical & Astrophysical Fluid Dynamics* **106**, 468 (2012).
- [46] P. H. Diamond, S. Itoh, K. Itoh, and T. Hahm, *Plasma Physics and Controlled Fusion* **47**, R35 (2005).
- [47] P. Guillon, G. Dif-Pradalier, Y. Sarazin, D. Hughes, and Ö. Gürçan, arXiv preprint arXiv:2511.10438 (2025).
- [48] V. S. L'vov, Y. L'vov, A. Newell, and V. Zakharov, *Physical Review E* **56**, 390 (1997).
- [49] M. Lesieur, *Turbulence in fluids: stochastic and numerical modelling*, Vol. 488 (Nijhoff Boston, MA, 1987).
- [50] M. Buzdicotti, H. Aluie, L. Biferale, and M. Linkmann, *Physical Review Fluids* **3**, 034802 (2018).
- [51] J. Marston and S. Tobias, *Annual Review of Fluid Mechanics* **55**, 351 (2023).
- [52] P. J. Schmid and D. S. Henningson, *Stability and transition in shear flows*, Vol. 142 (Springer Science & Business Media, 2012).
- [53] S. Galtier, *Physical Review E* **68**, 015301 (2003).

SUPPLEMENTARY INFORMATION

In this supplementary information, we detail the derivation of the mean-wave quasi-linear kinetic theory describing the interactions between a large-scale 2D flow and 3D inertial waves in rotating turbulence. We first establish the near-resonant conditions that select particular interaction types with increased rotation (§B). Wave-dominated interactions due to fast waves (in the sector called H), which conserve helicity by sign, are described in §C. Shear-dominated interactions due to slow waves (in the sector called A), which do not conserve helicity by sign, are described in §D. We derive analytical expressions for the wave energy flux through scales in this system in §E, and the resulting total energy transfer between the waves and the mean flow. Finally, we introduce a wavenumber cutoff above which wave-wave or eddy-eddy dominate over mean-fluctuation interactions, which controls the energy balance at low rotation and the transition to a regime of eddy turbulence (§F).

CONTENTS

A. Numerical setup	9
B. Mean-wave kinetic theory	10
C. Homochiral-wave interactions	13
D. Heterochiral interactions: governing equations	16
E. Flux coexistence due to rotation	17
1. Leading-order energy transfer	18
2. Exact energy transfer	22
a. Reynolds stress in Layers I	23
b. Summary of the exact Reynolds stress	24
3. Subleading corrections to the energy transfer	24
a. Layers II	24
b. Layers I	25
4. Numerical integration without cutoff	28
5. Analytical solution without cutoff	28
F. Cutting-off wave-wave and eddy-eddy interactions	30
1. Choice of cutoff	30
2. Numerical integration of the Reynolds stress with cutoff	31

Appendix A: Numerical setup

We consider the three-dimensional Navier-Stokes equations (3DNSE) written in the rotating frame,

$$\partial_t \mathbf{u} + \mathbf{u} \cdot \nabla \mathbf{u} = -2\Omega \mathbf{e}_z \times \mathbf{u} - \nabla p + \nu \nabla^2 \mathbf{u} + \nu_h \nabla^{2h} \mathbf{u} + \mathbf{f}, \quad (\text{A1})$$

in a periodic domain (L_x, L_y, L_z) of renormalized volume $\mathcal{V} = (L_x L_y L_z)/(2\pi)^3$. Forcing \mathbf{f} is such that $\langle \mathbf{f}_{\mathbf{p}}(t) \mathbf{f}_{\mathbf{q}}(t') \rangle = 2\epsilon \chi_{\mathbf{p}} \delta_{\mathbf{p}+\mathbf{q}} \delta(t-t')$, with correlation $\chi_{\mathbf{p}} = \delta_{p-k_f \pm 1}/(4\pi k_f^2 dk \mathcal{V})$ and ϵ the energy injection rate. Nondimensional Reynolds and Rossby numbers at the forcing scale $l_f \equiv 2\pi/k_f$ are defined as $Re = \epsilon^{1/3} k_f^{-4/3}/\nu$ and $Ro = \epsilon^{1/3} k_f^{2/3}/(2\Omega)$. We simulate Eq. (A1) with the pseudospectral code GHOST [29], with resolution $(N_x, N_y, N_z) = 128(L_x, L_y, L_z)/\pi$. The inertial range of the forward energy cascade is controlled by 8-order hyperviscosity $\nu_8 = 6 \times 10^{-29}$.

We decompose the 3D field into helical modes, $\mathbf{u}(\mathbf{x}, t) = \sum_{\mathbf{p}, s=\pm 1} \mathbf{h}_{\mathbf{p}}^s a_{\mathbf{p}}^s(t) e^{i\omega_{\mathbf{p}}^s t + i\mathbf{p} \cdot \mathbf{x}}$, with the helical basis

$$\mathbf{h}_{\mathbf{p}}^s = \frac{\mathbf{p} \times [\mathbf{p} \times \mathbf{e}_z] - ispp \times \mathbf{e}_z}{\sqrt{2}pp_{\perp}} = \frac{1}{\sqrt{2}pp_{\perp}} \begin{bmatrix} p_x p_z - ispp_y \\ p_z p_y + ispp_x \\ -p_x^2 - p_y^2 \end{bmatrix}, \quad (\text{A2})$$

with $\mathbf{p} = (p_x, p_y, p_z)$, $p = |\mathbf{p}|$ and $p_\perp^2 = p_x^2 + p_y^2$ [49]. This basis satisfies $i\mathbf{p} \times \mathbf{h}_\mathbf{p}^s = s\mathbf{h}_\mathbf{p}^s$ hence diagonalizes the curl operator. From such decomposition on the instantaneous field \mathbf{u} , we then measure the 3D-2D energy transfer

$$\Pi^{s_1, s_2} = - \sum_{|\mathbf{k}| < 5} \sum_{\mathbf{k} \in 2D, \mathbf{p}, \mathbf{q} \in 3D} \langle \mathbf{u}_\mathbf{k} \cdot (\mathbf{u}_\mathbf{p}^{s_1} \times \boldsymbol{\omega}_\mathbf{q}^{s_2}) \rangle \delta_{\mathbf{k}\mathbf{p}\mathbf{q}}, \quad (\text{A3})$$

Figure 1(d) in the main text shows the energy transfer due to homochiral waves, $\Pi^{++} + \Pi^{--}$, and due to heterochiral waves, $\Pi^{+-} + \Pi^{-+}$, for various values of Ro and Re . Note that we only decompose the energy flux with regard to the chiralities s_1, s_2 of the 3D modes, and do not further decompose contributions from the two chiralities of the 2D modes, as done in [40, 50]. Throughout this paper, we always refer to \mathbf{k} as being a 2D mode, and \mathbf{p} and \mathbf{q} as 3D waves.

Appendix B: Mean-wave kinetic theory

We consider a stationary mean flow $\mathbf{U} = \langle \mathbf{u} \rangle = U(y)\mathbf{e}_x$ consisting of two x -invariant jets, corresponding to the condensate in the rectangular domain $L_y = 2L_x$. The average $\langle \cdot \rangle$ denotes both ensemble and vertical average. In the following, we denote by

$$U' \equiv \sqrt{\frac{1}{L_y} \int (\partial_y U)^2 dy} \quad (\text{B1})$$

the root-mean-square shear rate, averaged over y . This defines a typical time scale $1/U'$ over which turbulent fluctuations interact with the condensate.

Interactions with the condensate dominate over eddy-eddy or wave-wave interactions: $1/U' \ll \tau_{nl}$, hence $\mathbf{u} \cdot \nabla \mathbf{u} \ll \mathbf{u} \cdot \nabla \mathbf{U}$. Under this quasi-linear (QL) approximation [51], the momentum equations for the mean flow and fluctuations \mathbf{u}' are written as

$$\partial_t U = -\partial_y \langle uv \rangle + \nu \partial_y^2 U = 0 \quad (\text{B2})$$

$$\partial_t \mathbf{u}' + U(y) \partial_x \mathbf{u}' = -\partial_y U v \mathbf{e}_x - 2\Omega \mathbf{e}_z \times \mathbf{u}' - \nabla p' + \mathbf{f}, \quad (\text{B3})$$

where u and v denote the x and y components of the fluctuating velocity \mathbf{u}' .

We decompose the fluctuation field as $\mathbf{u}'(\mathbf{x}, t) = \sum_{\mathbf{p}, s = \pm 1} \mathbf{h}_\mathbf{p}^s a_\mathbf{p}^s(t) e^{i\omega_\mathbf{p}^s t + i\mathbf{p} \cdot \mathbf{x}}$, where $a_\mathbf{p}^s(t)$ is the time-varying amplitude of a helical mode (\mathbf{p}, s) and $\omega_\mathbf{p}^s$ is the frequency of the corresponding inertial wave. We write the energy balance for the waves $e_\mathbf{p}^s = \frac{1}{2} \langle a_\mathbf{p}^s a_\mathbf{p}^{s*} \rangle$, as an energy increment at current time t , from an arbitrary $t = 0$,

$$\frac{e_\mathbf{p}^s(t) - e_\mathbf{p}^s(0)}{t} = \frac{1}{2t} \sum_{\mathbf{q}, \mathbf{k}, \bar{s}} \left[V_{\mathbf{p}\mathbf{k}\mathbf{q}}^{s\bar{s}} U_\mathbf{k}^* \langle a_\mathbf{p}^{s*} a_\mathbf{q}^{\bar{s}*} \rangle(t) e^{-i\omega_{\mathbf{p}\mathbf{q}}^{s\bar{s}} t} \right] \delta_{\mathbf{k}\mathbf{p}\mathbf{q}} + c.c. + \epsilon \chi_\mathbf{p}^s \quad (\text{B4})$$

where

$$\omega_{\mathbf{p}\mathbf{q}}^{s\bar{s}} \equiv \omega_\mathbf{p}^s + \omega_\mathbf{q}^{-s} = s2\Omega p_z \left(\frac{1}{p} + \frac{1}{q} \right) \quad (\text{B5})$$

We now assume that wave-mean flow interactions occur on a typical time scale of the order of $1/U'$, so that over a much shorter time scale, of order $t \ll 1/U'$, the wave amplitude correlators can be assumed constant. Thus, performing a partial time average up to time $t \ll 1/U'$,

$$\begin{aligned} \frac{e_\mathbf{p}^s(t) - e_\mathbf{p}^s(0)}{t} &= \frac{1}{2} \sum_{\mathbf{q}, \mathbf{k}, \bar{s}} \left[V_{\mathbf{p}\mathbf{k}\mathbf{q}}^{s\bar{s}} U_\mathbf{k}^* \langle a_\mathbf{p}^{s*} a_\mathbf{q}^{\bar{s}*} \rangle \frac{1}{t} \int_0^t e^{-i\omega_{\mathbf{p}\mathbf{q}}^{s\bar{s}} t'} dt' \right] \delta_{\mathbf{k}\mathbf{p}\mathbf{q}} + c.c. + \epsilon \chi_\mathbf{p}^s \\ &\approx \frac{1}{2} \sum_{\mathbf{q}, \mathbf{k}, \bar{s}} \frac{1 - e^{-i\omega_{\mathbf{p}\mathbf{q}}^{s\bar{s}} t}}{i\omega_{\mathbf{p}\mathbf{q}}^{s\bar{s}} t} \left[V_{\mathbf{p}\mathbf{k}\mathbf{q}}^{s\bar{s}} U_\mathbf{k}^* \langle a_\mathbf{p}^{s*} a_\mathbf{q}^{\bar{s}*} \rangle \right] \delta_{\mathbf{k}\mathbf{p}\mathbf{q}} + c.c. + \epsilon \chi_\mathbf{p}^s \\ &= \frac{1}{2} \sum_{\mathbf{q}, \mathbf{k}, \bar{s}} \Delta^{s\bar{s}}(t) \left[V_{\mathbf{p}\mathbf{k}\mathbf{q}}^{s\bar{s}} U_\mathbf{k}^* \langle a_\mathbf{p}^{s*} a_\mathbf{q}^{\bar{s}*} \rangle \right] \delta_{\mathbf{k}\mathbf{p}\mathbf{q}} + c.c. + \epsilon \chi_\mathbf{p}^s + o\left(\frac{U'}{\Omega}\right) \end{aligned} \quad (\text{B6})$$

where

$$\Delta_{\mathbf{p}}^{s\bar{s}}(t) \equiv \frac{1 - e^{-i\omega_{\mathbf{p}\mathbf{q}}^{s\bar{s}}t}}{i\omega_{\mathbf{p}\mathbf{q}}^{s\bar{s}}t}. \quad (\text{B7})$$

Here we will generally consider interactions between waves of opposite chiralities due to their coupling with the condensate mode \mathbf{k} , assuming $\langle a_{\mathbf{p}}^s a_{\mathbf{q}}^{-s} \rangle \neq 0$, and follow the same procedure as in [30]. Note that such correlations are absent initially, as our forcing does not directly correlate waves of opposite polarity, ($\langle f_{\mathbf{p}}^s f_{\mathbf{q}}^{-s} \rangle = 0$). An additional equation is therefore needed to close the system, given by the evolution of the correlation between opposite polarity modes $\langle a_{\mathbf{p}}^{s*} a_{\mathbf{p}}^{-s} \rangle$

$$\frac{\langle a_{\mathbf{p}}^{s*} a_{\mathbf{p}}^{-s} \rangle(t) - \langle a_{\mathbf{p}}^{s*} a_{\mathbf{p}}^{-s} \rangle(0)}{t} = \sum_{\mathbf{q}, \mathbf{k}, s} \left[U_{\mathbf{k}}^* V_{\mathbf{p}\mathbf{k}\mathbf{q}}^{-s, \bar{s}} \langle a_{\mathbf{p}}^s a_{\mathbf{q}}^{\bar{s}} \rangle^* \Delta^{-s, \bar{s}} + U_{\mathbf{k}} V_{\mathbf{p}\mathbf{k}\mathbf{q}}^{s\bar{s}*} \langle a_{\mathbf{p}}^{-s} a_{\mathbf{q}}^{\bar{s}} \rangle \Delta^{s\bar{s}*} \right] \delta_{\mathbf{k}\mathbf{p}\mathbf{q}} \quad (\text{B8})$$

Note that if heterochiral wave interactions, such that $\bar{s} = -s$, are here set to zero, the cross-helicity correlators would not get spontaneously generated.

Similarly to [30], we approximate the oscillating factor in equations (B6) and (B17) as

$$\Delta_{\mathbf{p}}^{s\bar{s}}(t) = \frac{1 - e^{-i\omega_{\mathbf{p}\mathbf{q}}^{s\bar{s}}t}}{i\omega_{\mathbf{p}\mathbf{q}}^{s\bar{s}}t} \approx F_{\mathbf{p}\mathbf{q}} \left(\frac{U'}{\Omega} \right), \quad (\text{B9})$$

with the simplest choice of a filter being a step function

$$F_{\mathbf{p}\mathbf{q}} = \Theta \left(1 - \frac{|\omega_{\mathbf{p}\mathbf{q}}^{s\bar{s}}|}{U'} \right) \quad (\text{B10})$$

where Θ denotes the Heaviside function, leading to the near-resonant condition

$$\omega_{\mathbf{p}}^s + \omega_{\mathbf{q}}^s < U' \quad (\text{B11})$$

for homochiral-wave interactions.

For cross-helicity interactions $\bar{s} = -s$, using scale separation between k and p and recalling that $\mathbf{q} = -\mathbf{p} - \mathbf{k}$ we get $\omega_{\mathbf{p}\mathbf{q}}^{s, -s} \simeq 2\omega_{\mathbf{p}}^s = 4s\Omega p_z/p$. Thus, the step-function approximation (B9) results in a condition delimiting near-resonant from off-resonant interactions:

$$\Delta_{\mathbf{p}}^{s, -s}(t) = \frac{1 - e^{i\omega_{\mathbf{p}\mathbf{q}}^{s, -s}t}}{i\omega_{\mathbf{p}\mathbf{q}}^{s, -s}t} \approx \begin{cases} 1, & \omega_{\mathbf{p}}^s + \omega_{\mathbf{q}}^{-s} \leq U' \Leftrightarrow \frac{4p_z}{p} \leq \frac{U'}{\Omega} \\ 0, & \omega_{\mathbf{p}}^s + \omega_{\mathbf{q}}^{-s} > U' \Leftrightarrow \frac{4p_z}{p} > \frac{U'}{\Omega} \end{cases} \quad (\text{B12})$$

Conditions (B12) lead to the definition of two separate sectors A and H:

$$\begin{cases} \text{Sector H: } 2\omega_{\mathbf{p}} > U' \Leftrightarrow \frac{4p_z}{p} > \frac{U'}{\Omega} \text{ (homochiral interactions)} \\ \text{Sector A: } 2\omega_{\mathbf{p}} < U' \Leftrightarrow \frac{4p_z}{p} \leq \frac{U'}{\Omega} \text{ (all interactions),} \end{cases} \quad (\text{B13})$$

For modes \mathbf{p} in sector H, heterochiral-wave interactions decorrelate ($\Delta_{\mathbf{p}}^{s, -s} \approx 0$) and only homochiral-wave interactions ($\bar{s} = s$) are present. For modes in sector A, on the other hand, both types of interactions are allowed by the resonance condition and these modes experience the full 3D QL dynamics. Note that the resonant condition for homochiral-wave interactions (B11) is less restrictive than that for heterochiral-wave interactions (B12), and that the former becomes restrictive for modes in sector H at sufficiently high rotation rates. At large rotation ($\frac{U'}{\Omega} < l_f/(L_y)$), modes for which $\Delta_{\mathbf{p}}^{s\bar{s}} \approx 0$ at the forcing scale do not interact with the condensate, as discussed in [30], and in the QL dynamics are treated as if unforced.

Note also that there is a lower bound for the time t we need to consider here: the oscillations of the waves will be felt by the system (meaning that some interactions will average out to zero) only for times much larger than $1/\max(\omega_{\mathbf{p}\mathbf{q}}^{s\bar{s}}) = 1/4\Omega$, which occurs in interactions between opposite-helicity waves, $s = -\bar{s}$. Hence, such an expansion makes sense for $1/4\Omega \ll t \ll 1/U'$, requiring a sufficient time-scale separation. Thus, the kinetic equation that we derive is an expansion in $U'/4\Omega$ (the ratio between the wave and non-linear time scale), where we keep the leading order term $O(U'/4\Omega)$. Condition $U'/4\Omega < 1$ is required for the existence of Sector H.

We now consider the lowest complex-conjugate modes $k_y = \pm 2\pi/L_y$ for the condensate $U_{\mathbf{k}} = \frac{U'}{i\sqrt{2k_y}}$, and expand the coefficients in the limit $Lk_f \gg 1$:

$$\begin{aligned} V_{\mathbf{pkq}}^{ss} &= -ip_x - sk_y \left(\frac{p_x^2 p_z}{p_\perp^2 p} + \frac{p_z}{2p} \right) - ik_y \frac{p_x p_y}{2p^2} + O\left(\frac{k_y^2}{p^2}\right), & V_{\mathbf{pkq}}^{s,-s} &= ik_y V_{\mathbf{p}}^{s,-s} + O\left(\frac{k_y^2}{p^2}\right), \\ &= -ip_x - 2ik_y V_{\mathbf{p}}^{ss} + O\left(\frac{k_y^2}{p^2}\right), \end{aligned} \quad (\text{B14})$$

where we have defined

$$V_{\mathbf{p}}^{ss} \equiv -is \frac{p_z}{p} \left(1 + \frac{2p_x^2}{p_\perp^2} \right) + \frac{p_x p_y}{p^2}, \quad V_{\mathbf{p}}^{s,-s} \equiv \frac{p_x p_y}{p^2} \left(1 + \frac{p_z^2}{p_\perp^2} \right) + is \frac{p_z}{p} \left(1 - \frac{2p_x^2}{p_\perp^2} \right). \quad (\text{B15})$$

When considering condition (B12) for heterochiral-wave interactions, and assuming that homochiral waves resonate with the condensate ($\omega_{\mathbf{p}}^s + \omega_{\mathbf{q}}^s < U'$), we obtain the coupled equations

$$\partial_t e_{\mathbf{p}}^s = \frac{U'}{\sqrt{2}} \left(\left[p_x \partial_{p_y} + \Re[V_{\mathbf{p}}^{ss}] \right] \Phi_{\mathbf{pk}}^s - \mathbb{1}_{\mathbf{p} \in A} \Re[V_{\mathbf{p}}^{s,-s} \Psi_{\mathbf{pk}}^{s,-s*}] \right) + \epsilon \chi_{\mathbf{p}}^s \quad (\text{B16})$$

$$\partial_t \langle a_{\mathbf{p}}^{s*} a_{\mathbf{p}}^{-s} \rangle = 2 \frac{U'}{\sqrt{2}} \left(\left[p_x \partial_{p_y} + V_{\mathbf{p}}^{ss} \right] (\Psi_{\mathbf{pk}}^{s,-s*} + \Psi_{\mathbf{pk}}^{-s,s}) - \mathbb{1}_{\mathbf{p} \in A} V_{\mathbf{p}}^{s,-s*} (\Phi_{\mathbf{pk}}^{s*} + \Phi_{\mathbf{pk}}^{-s}) \right), \quad (\text{B17})$$

with correlators

$$\Phi_{\mathbf{pk}}^s \equiv \frac{\langle a_{\mathbf{p}}^s a_{-\mathbf{p}+\mathbf{k}}^s \rangle + \langle a_{\mathbf{p}}^s a_{-\mathbf{p}-\mathbf{k}}^s \rangle}{2} = \frac{\langle a_{\mathbf{p}}^s a_{-\mathbf{p}+\mathbf{k}}^s \rangle + c.c.}{2} + O\left(\frac{k_y}{p}\right) \quad (\text{B18})$$

and

$$\Psi_{\mathbf{pk}}^{s,-s} \equiv \frac{\langle a_{\mathbf{p}}^s a_{-\mathbf{p}+\mathbf{k}}^{-s} \rangle + \langle a_{\mathbf{p}}^s a_{-\mathbf{p}-\mathbf{k}}^{-s} \rangle}{2}. \quad (\text{B19})$$

Note that $\Im(\Phi_{\mathbf{pk}}) = O(k_y/p)$, while $\Psi_{\mathbf{pk}} \in \mathbb{C}$ at the leading order in k_y/p .

The wave kinetic equations (B16)-(B17) are coupled with the mean-flow equation (B2), obtained by Reynolds averaging over time $T \gg 1/U'$ and over z , in a time window where the ensemble-averaged correlator $\langle a_{\mathbf{p}}^s a_{\mathbf{q}}^{s'} \rangle$ is stationary. The total energy transfer is

$$T_{3\text{D}-2\text{D}} = \sum_{\mathbf{p}, s, \bar{s}} U'_{-\mathbf{k}} \langle u_{\mathbf{p}}^s v_{-\mathbf{p}+\mathbf{k}}^{\bar{s}} \rangle + U'_{\mathbf{k}} \langle u_{\mathbf{p}}^s v_{-\mathbf{p}-\mathbf{k}}^{\bar{s}} \rangle = \frac{\mathcal{V}U'}{\sqrt{2}} \int d\mathbf{p} \sum_{s, \bar{s}=\pm 1} \langle uv \rangle_{\mathbf{pk}}^{s\bar{s}} \quad (\text{B20})$$

Note that the $1/\sqrt{2}$ prefactor is an unimportant normalization factor due to our choice of definition for U' (B1). In Eq. (B20) the Reynolds stress due to homochiral interactions is

$$\langle uv \rangle_{\mathbf{pk}}^{ss} \equiv \frac{1}{2} \left(\langle u_{\mathbf{p}}^s v_{-\mathbf{p}-\mathbf{k}}^s \rangle + \langle u_{\mathbf{p}}^s v_{-\mathbf{p}+\mathbf{k}}^s \rangle \right) + c.c. = -\frac{p_x p_y}{p^2} \Phi_{\mathbf{pk}}^s + O\left(\frac{k_y}{p}\right) \quad (\text{B21})$$

where in the last line we used that $h_{\mathbf{p},x}^{-s} h_{-\mathbf{p}-\mathbf{k},y}^{-s} = h_{\mathbf{p},x}^{-s} h_{-\mathbf{p},y}^{-s} + O(k_y/p) = -\frac{p_x p_y}{2p^2} + is \frac{p_z}{2p} + O(k_y/p)$, that $\Phi_{\mathbf{pk}}^s = \Phi_{\mathbf{p},-\mathbf{k}}^s$ and that the imaginary part of the correlator is subleading:

$$\begin{aligned} 2\Im \left[\langle a_{\mathbf{p}}^s a_{-\mathbf{p}+\mathbf{k}}^s \rangle + \langle a_{\mathbf{p}}^s a_{-\mathbf{p}-\mathbf{k}}^s \rangle \right] &= \langle a_{\mathbf{p}}^s a_{-\mathbf{p}+\mathbf{k}}^s \rangle + \langle a_{\mathbf{p}}^s a_{-\mathbf{p}-\mathbf{k}}^s \rangle - c.c. \\ &= \langle a_{\mathbf{p}}^s a_{-\mathbf{p}+\mathbf{k}}^s \rangle - \langle a_{\mathbf{p}+\mathbf{k}}^s a_{-\mathbf{p}}^s \rangle + \langle a_{\mathbf{p}}^s a_{-\mathbf{p}-\mathbf{k}}^s \rangle - \langle a_{\mathbf{p}-\mathbf{k}}^s a_{-\mathbf{p}}^s \rangle \\ &= -k_y \partial_{p_y} \langle a_{\mathbf{p}-\mathbf{k}}^s a_{-\mathbf{p}}^s \rangle + k_y \partial_{p_y} \langle a_{\mathbf{p}-\mathbf{k}}^s a_{-\mathbf{p}}^s \rangle \\ &= o\left(\frac{k_y}{p}\right), \end{aligned} \quad (\text{B22})$$

using a Taylor expansion in each correlator.

The contribution of heterochiral interactions to the Reynolds stress is given by

$$\begin{aligned}
\langle uv \rangle_{\mathbf{pk}}^{s,-s} &\equiv \langle u_{\mathbf{p}}^s v_{-\mathbf{p}+\mathbf{k}}^{-s} + u_{\mathbf{p}}^s v_{-\mathbf{p}-\mathbf{k}}^{-s} \rangle \\
&= \frac{1}{T} \int_0^T dt \left(h_{\mathbf{p},x}^{-s} h_{-\mathbf{p}+\mathbf{k},y}^s \langle a_{\mathbf{p}}^{-s*} a_{-\mathbf{p}+\mathbf{k}}^{s*} \rangle e^{i(\omega_{\mathbf{p}}^s + \omega_{-\mathbf{p}+\mathbf{k}}^{-s})t} + (\mathbf{k} \rightarrow -\mathbf{k}) \right) \\
&\simeq \Re(V_{\mathbf{p}}^{s,-s} \Psi_{\mathbf{pk}}^{s,-s}) + O\left(\frac{k_y}{p}\right)
\end{aligned} \tag{B23}$$

for heterochiral modes in Sector A (and zero for modes in sector H). This heterochiral correlator contributes to the total Reynolds stress in Eq. (B20), in addition to the contribution of homochiral waves via Eq. (B21).

Now we can recognize in the RHS of Eq. (B16) the heterochiral Reynolds-stress correlator (B23), as expected from the conservation of energy in the system including the mean flow. The energy balance Eq. (B16) is therefore of the form

$$\partial_t e_{\mathbf{p}}^s + \partial_{p_y} \Pi_{\mathbf{p}}^s = -\frac{U'}{\sqrt{2}} \left(\langle uv \rangle_{\mathbf{pk}}^{ss} + \langle uv \rangle_{\mathbf{pk}}^{s,-s} \right) + \epsilon \chi_{\mathbf{p}}^s \tag{B24}$$

This energy balance is valid in both Sectors A and H. Note that in steady state, Eq. (B24) reflects the balance between the wave energy flux and the transfer to the mean-flow:

$$\partial_{p_y} \Pi_{\mathbf{p}}^s = -\frac{U'}{\sqrt{2}} \langle uv \rangle_{\mathbf{pk}} + \epsilon \chi_{\mathbf{p}}^s, \tag{B25}$$

with the total Reynolds stress correlator $\langle uv \rangle_{\mathbf{pk}} = \langle uv \rangle_{\mathbf{pk}}^{ss} + \langle uv \rangle_{\mathbf{pk}}^{s,-s}$. Away from the forcing scale ($\chi_{\mathbf{p}}^s = 0$), waves either lose energy to the 2D flow (the wave energy flux $\Pi_{\mathbf{k}}^s$ decreases with p_y and the transfer to the 2D flow $\frac{U'}{\sqrt{2}} \langle uv \rangle_{\mathbf{pk}} > 0$), or gain energy from the 2D flow.

Now focusing on helicity, multiplying (B24) by sp leads to the spectral helicity balance

$$\partial_t (s p e_{\mathbf{p}}^s) + \partial_{p_y} (s p \Pi_{\mathbf{p}}^s) = -\mathbb{1}_{\mathbf{p} \in A} s p \frac{U'}{\sqrt{2}} \langle uv \rangle_{\mathbf{pk}}^{s,-s} + s p \epsilon \chi_{\mathbf{p}}^s. \tag{B26}$$

Due to scale separation $k_y/p \ll 1$, the helicity transfer between the waves and the mean flow can be neglected. Indeed, decomposing the condensate mode \mathbf{k} into its two chiralities, the helicity transfer with the waves is

$$\mathcal{H}_{\mathbf{k}} = k(\mathcal{E}_{\mathbf{k}}^+ - \mathcal{E}_{\mathbf{k}}^-) \tag{B27}$$

with $\mathcal{E}_{\mathbf{k}}^{\pm}$ the energy transfer between the waves and the 2D mode of polarity ± 1 . $\mathcal{E}_{\mathbf{k}}^{\pm}$ can be explicitly written from the helical decomposition of the wave field, but this does not matter for the argument. Scale selection $k_y/k_f \ll 1$ implies that the 2D-3D helicity exchange (B27) is negligible: at most, $\mathcal{H}_{\mathbf{k}} = O(k_y \epsilon)$, in the (unexpected) case where one mean-flow polarity absorbs all the wave energy, hence $\mathcal{H}_{\mathbf{k}} \ll k_f \epsilon^s$, the amount of helicity injected in each wave sector s . Therefore, the waves conserve their helicity separately, independently of the type of condensate-wave interaction (homochiral or heterochiral). Note that conservation of total helicity of the fluctuations implies that

$$\langle uv \rangle_{\mathbf{pk}}^{s,-s} = \langle uv \rangle_{\mathbf{pk}}^{-s,s} \tag{B28}$$

and we see that the first term on the RHS of Eq. (B26) corresponds to the change in helicity of sign(s) due to interactions with modes of opposite helicity, mediated by the condensate. In particular, if there is a finite (and positive) energy flux at arbitrary large scales p , $\lim_{p \rightarrow \infty} \Pi_{\text{adv}}^s > 0$, then this flux serves as the source for the generation of helicity of sign s . The helicity flux $s p \Pi^s$ must therefore increase with p and be of sign s . From Eq. (B26), this implies that $\frac{U'}{\sqrt{2}} \langle uv \rangle_{\mathbf{pk}}^{s,-s} < 0$ for large enough p , which in turn implies that the cross-helicity Reynolds stress acts on the mean flow to extract energy from it.

Therefore, in the presence of cross-helicity interactions, modes of positive and negative helicity extract energy from the mean flow symmetrically, to compensate for the increase of helicity of a particular sign due to the p_y energy flux.

Appendix C: Homochiral-wave interactions

Here we focus on Sector H, where heterochiral interactions are off-resonant, hence $\langle a_{\mathbf{p}}^s a_{-\mathbf{p}+\mathbf{k}}^{-s} \rangle = 0$. The procedure is exactly that in [30]. Due to the presence of two sign-definite invariants in this sector (energy and single-sign helicity

$H^s \equiv \sum spe_p^s$, the steady-state solution is straightforward. Equation (B16) for $\mathbf{p} \in H$ can be written in steady state in the form

$$\partial_{p_y} \left(-sp \frac{U' p_x}{\sqrt{2}} \Phi_{\mathbf{p}\mathbf{k}}^s \right) \equiv \partial_{p_y} (\Pi_{H^s}) = sp \epsilon \chi_p^s \quad (\text{C1})$$

which is solved by:

$$\begin{aligned} \Phi_{\mathbf{p}\mathbf{k}}^s &= -\frac{\sqrt{2}\epsilon}{U' p_x} \int_{-\infty}^{p_y} \frac{q}{p} \chi_q^s dq_y \quad \text{for } U' p_x < 0 \ (dq_y > 0); \\ \Phi_{\mathbf{p}\mathbf{k}}^s &= -\frac{\sqrt{2}\epsilon}{U' p_x} \int_{\infty}^{p_y} \frac{q}{p} \chi_q^s dq_y \quad \text{for } U' p_x > 0 \ (dq_y < 0). \end{aligned} \quad (\text{C2})$$

where we have used different boundary conditions depending on the sign of $U' p_x$:

$$\Pi_{H^s}(p_y \rightarrow -\infty) = 0 \quad \text{for } U' p_x < 0 \quad (\text{C3})$$

$$\Pi_{H^s}(p_y \rightarrow \infty) = 0 \quad \text{for } U' p_x > 0 \quad (\text{C4})$$

implying that for $U' p_x < 0$ ($U' p_x > 0$) the flux of helicity is from the forcing scale to $p_y \rightarrow \infty$ ($p_y \rightarrow -\infty$), i.e. to positive (negative) p_y .

Solution (C2) is simplified when $\chi_p^s = \chi_p^{-s} = \delta(p - k_f)/(8\pi k_f^2 \mathcal{V})$ and leads to the small-scale energy flux:

$$\Pi_{\mathbf{p}}^s \equiv \frac{-U' p_x}{\sqrt{2}} \Phi_{\mathbf{p}\mathbf{k}}^s = \begin{cases} 0 & \text{if } \sigma p_y < -p_y^f \\ \frac{\sigma \epsilon_{p_x, p_z} k_f}{2} \frac{k_f}{p} & \text{if } -p_y^f < \sigma p_y < p_y^f \\ \sigma \epsilon_{p_x, p_z} \frac{k_f}{p} & \text{if } \sigma p_y > p_y^f \end{cases} \quad (\text{C5})$$

with $\sigma \equiv \text{sgn}(-U' p_x)$ the relative sign of the shear and

$$\begin{aligned} \epsilon_{p_x, p_z}^s &\equiv \int_{-\infty}^{\infty} \chi_q^s F_{\mathbf{q}-\mathbf{k}-\mathbf{q}} dq_y = \frac{1}{8\pi k_f^2 \mathcal{V}} \int_{-\infty}^{\infty} \delta(q - k_f) F_{\mathbf{p}\mathbf{q}} dq_y \\ &= \frac{1}{8\pi k_f^2 \mathcal{V}} \frac{2k_f}{p_y} F_{k_f} = \frac{\epsilon F_{k_f}}{4\pi k_f \mathcal{V} \sqrt{k_f^2 - p_x^2 - p_z^2}} \end{aligned} \quad (\text{C6})$$

the energy injection rate in each (p_x, p_z) line in sector s . We have also defined

$$F_{k_f} \equiv F_{\mathbf{p}, -\mathbf{k}-\mathbf{k}} \delta_{p-k_f} \quad (\text{C7})$$

equal to the resonant filter (B10) evaluated at the forcing scale. Here we have multiplied the energy injection rate by the filter to take into account the fact that some of the modes decouple from the condensate, if $\Delta^{ss} \approx 0 \Leftrightarrow \omega_{\mathbf{p}\mathbf{q}}^{ss} \delta_{p-k_f} < U'$ at the forcing scale (which implies that $\Delta_{\mathbf{p}}^{s,-s} \approx 0$). Such modes only interact with other 3D waves are then treated as if they are unforced in the QL system. Then, $\Phi_{\mathbf{p}\mathbf{k}}^s = 0$ and the corresponding Reynolds stress is zero. The decoupling of 2D-3D interactions as $\Omega \rightarrow \infty$ is discussed in [30].

Solution (C5) reflects the conservation of helicity within each polar sector: $p\Pi^s = k_f \epsilon_{p_x, p_z}^s$ with the energy flux $\Pi^s = -U' p_x \Phi_{\mathbf{p}\mathbf{k}}^s$. This shows that the conservation of helicity by sign imposes a decaying energy flux to small scales, $\Pi^s \sim k_f/p \epsilon_{p_x, p_z}^s$. The sign of Π^s depends on the sign of $-U' p_x p_y$, as follows from the choice of boundary conditions (C4): it is positive when $p_y > 0$ and $U' p_x < 0$.

The corresponding Reynolds transfer is written as

$$\frac{U'}{\sqrt{2}} \langle uv \rangle_{\mathbf{p}\mathbf{k}} = -\frac{U'}{\sqrt{2}} \frac{p_x p_y}{p^2} (\Phi_{\mathbf{p}\mathbf{k}}^+ + \Phi_{\mathbf{p}\mathbf{k}}^-) \quad (\text{C8})$$

$$= \begin{cases} 0 & \text{if } \sigma p_y < -p_y^f \\ \frac{\sigma \epsilon_{p_x, p_z} k_f p_y}{2} \frac{k_f p_y}{p^3} & \text{if } -p_y^f < \sigma p_y < p_y^f \\ \sigma \epsilon_{p_x, p_z} \frac{k_f p_y}{p^3} & \text{if } \sigma p_y > p_y^f \end{cases} \quad (\text{C9})$$

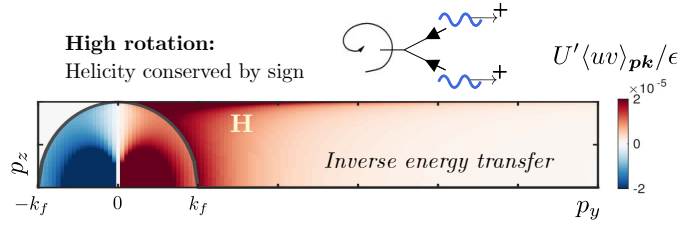


FIG. 5: Reynolds stress in the spectral plane ($p_y, p_z, p_x = 8\pi/L_x$), computed when interactions are homochiral (Sector H). This corresponds to the high-rotation regime. Advection by the shear flow generates a decaying forward flux of wave energy, which is transferred to the shear flow ($U'\langle uv\rangle_{\mathbf{pk}} > 0$).

with

$$\epsilon_{p_x, p_z} = \epsilon_{p_x, p_z}^+ + \epsilon_{p_x, p_z}^- = \frac{\epsilon F_{k_f}}{2\pi \sqrt{k_f^2 - p_x^- p_z^2} k_f \mathcal{V}} \quad (\text{C10})$$

the total energy injected in the (p_x, p_z) layer. This solution is shown in Fig. 5. Importantly, $\frac{U'}{\sqrt{2}}\langle uv\rangle_{\mathbf{pk}}$ is positive when $\sigma p_y > 0$: energy goes from the waves to the 2D condensate.

Appendix D: Heterochiral interactions: governing equations

System (B16)-(B17) when all modes \mathbf{p} are in Sector A describes *rotation-free* interactions between 3D modes, excited at scale l_f , and an imposed large-scale mean flow $\mathbf{U}(y)$. This is due to the frequencies of 3D modes in this sector being too slow, so that $\Delta_{\mathbf{p}}^{\pm} \approx 1$ and rotation has no effect on the QL dynamics at leading order. For these modes, the same dynamical system would be obtained if Ω were put to 0 in Eq. (B3).

However, the helical basis does not diagonalize the stationary system of correlators $\Phi_{\mathbf{p}}^s, \Psi_{\mathbf{p}}^{\pm}$. Instead, the system can be triangularized, and possibly solved analytically, when formulating the fluid equations in terms of primary variables, as is classically done in mean-fluctuation descriptions of shear flows [34, 52]. In this section we will present the solution for the energy flux and Reynolds stress for this non-rotating, directly forced case. This solution will be useful for the treatment of modes in Sector A, which also exhibit such dynamics and can either be directly forced, or receive their energy through a flux in p space, coming from modes in the homochiral sector.

We consider a non-rotating system of mean flow $\mathbf{U} = U(y)\mathbf{e}_x$ with a *given mean shear rate* U' , and 3D perturbations $[u, v, w](x, y, z)$ such that $\mathbf{u} \cdot \nabla \mathbf{u} \ll \mathbf{u} \cdot \nabla \mathbf{U}$, which obeys the Rayleigh equations

$$\partial_t \begin{bmatrix} \nabla^2 v \\ \eta \end{bmatrix} = \begin{bmatrix} -(U\nabla^2 - \partial_y^2 U)\partial_x & 0 \\ -U'\partial_z & -U\partial_x \end{bmatrix} \begin{bmatrix} v \\ \eta \end{bmatrix} + \begin{bmatrix} \nabla^2 f_y \\ (\nabla \times \mathbf{f})_y \end{bmatrix} \quad (\text{D1})$$

with $\eta \equiv (\nabla \times \mathbf{u})_y$ the y -component of vorticity (see e.g [34]). Restricting Eq. (D1) to our sinusoidal mean flow $U(y) = U' L_y / (\sqrt{2}\pi) \sin(2\pi y / L_y)$, $U_{\mathbf{k}} = \frac{U'}{i\sqrt{2}k_y}$ and using scale separation $L_y k_f \gg 1$ (consequently, $\partial_y^2 U \ll U\nabla^2$), we obtain the simplified system in Fourier space:

$$\partial_t (p^2 v_{\mathbf{p}}) = \frac{p_x U'}{\sqrt{2}k_y} \left[|-\mathbf{p} - \mathbf{k}|^2 v_{-\mathbf{p}-\mathbf{k}}^* - |-\mathbf{p} + \mathbf{k}|^2 v_{-\mathbf{p}+\mathbf{k}}^* \right] + p^2 f_{\mathbf{p},y} \quad (\text{D2})$$

$$\partial_t \eta_{\mathbf{p}} = \frac{U'}{\sqrt{2}} \left[\frac{p_x}{k_y} (\eta_{-\mathbf{p}-\mathbf{k}}^* - \eta_{-\mathbf{p}+\mathbf{k}}^*) - ip_z (v_{-\mathbf{p}-\mathbf{k}}^* + v_{-\mathbf{p}+\mathbf{k}}^*) \right] + g_y \quad (\text{D3})$$

with $k_y = 2\pi/L_y$ and $g_y = ip_z f_{\mathbf{p},x} - ip_x f_{\mathbf{p},z}$ and where we have used that $p_x = -q_x, p_y = -q_y \pm k_y, p_z = -q_z$.

We now write the equation for the ensemble-averaged cross-flow energy $\langle |v_{\mathbf{p}}|^2 \rangle$, velocity-vorticity correlation $\langle \eta_{\mathbf{p}} v_{-\mathbf{p}} \rangle$ and cross-flow enstrophy $\langle |\eta_{\mathbf{p}}|^2 \rangle$ at $O(k_y/p)$:

$$\partial_t \frac{\langle |v_{\mathbf{p}}|^2 \rangle}{2} = \frac{U'}{\sqrt{2}} \left[p_x \partial_{p_y} + \frac{4p_x p_y}{p^2} \right] \langle vv \rangle_{\mathbf{p}\mathbf{k}} + \epsilon \chi_{\mathbf{p},y} \quad (\text{D4})$$

$$\partial_t \frac{\langle \eta_{\mathbf{p}} v_{-\mathbf{p}} \rangle}{2} = \frac{U'}{\sqrt{2}} \left(\left[p_x \partial_{p_y} + 2 \frac{p_x p_y}{p^2} \right] \langle \eta v \rangle_{\mathbf{p}\mathbf{k}} - ip_z \langle vv \rangle_{\mathbf{p}\mathbf{k}} \right) \quad (\text{D5})$$

$$\partial_t \frac{\langle |\eta_{\mathbf{p}}|^2 \rangle}{2} = \frac{U'}{\sqrt{2}} \left(p_x \partial_{p_y} \langle \eta \eta \rangle_{\mathbf{p}\mathbf{k}} - 2p_z \Im \langle \eta v \rangle_{\mathbf{p}\mathbf{k}} \right) + \epsilon p^2 \chi_{\mathbf{p},y} \quad (\text{D6})$$

where we have defined

$$\langle vv \rangle_{\mathbf{p}\mathbf{k}} \equiv \frac{1}{2} \left(\langle v_{\mathbf{p}} v_{-\mathbf{p}+\mathbf{k}} \rangle + \langle v_{\mathbf{p}} v_{-\mathbf{p}-\mathbf{k}} \rangle \right), \quad \langle \eta v \rangle_{\mathbf{p}\mathbf{k}} \equiv \frac{1}{2} \left(\langle \eta_{\mathbf{p}} v_{-\mathbf{p}+\mathbf{k}} \rangle + \langle \eta_{\mathbf{p}} v_{-\mathbf{p}-\mathbf{k}} \rangle \right), \quad \langle \eta \eta \rangle_{\mathbf{p}\mathbf{k}} \equiv \frac{1}{2} \left(\langle \eta_{\mathbf{p}} \eta_{-\mathbf{p}+\mathbf{k}} \rangle + \langle \eta_{\mathbf{p}} \eta_{-\mathbf{p}-\mathbf{k}} \rangle \right) \quad (\text{D7})$$

and used that $\langle vv \rangle_{\mathbf{p}\mathbf{k}}^* = \langle vv \rangle_{\mathbf{p}\mathbf{k}}$ since $\langle v_{\mathbf{p}} v_{-\mathbf{p}+\mathbf{k}} \rangle = \langle v_{-\mathbf{p}} v_{\mathbf{p}+\mathbf{k}} \rangle + O(k_y/p)$, as well as

$$\begin{aligned} \langle v_{\mathbf{p}} v_{-\mathbf{p}-\mathbf{k}} \rangle &= \langle v_{-\mathbf{p}} v_{\mathbf{p}-\mathbf{k}} \rangle + O(k_y/p), & \langle v_{\mathbf{p}} v_{-\mathbf{p}-\mathbf{k}} \rangle &= \langle v_{-\mathbf{p}} v_{\mathbf{p}-\mathbf{k}} \rangle + O(k_y/p), & \langle \eta_{\mathbf{p}} v_{-\mathbf{p}+\mathbf{k}} \rangle &= \langle \eta_{\mathbf{p}-\mathbf{k}} v_{-\mathbf{p}} \rangle + O(k_y/p), \\ k_y \partial_{p_y} \langle \eta v \rangle_{\mathbf{p}\mathbf{k}} &= \langle \eta_{\mathbf{p}+\mathbf{k}} v_{-\mathbf{p}} \rangle - \langle \eta_{\mathbf{p}} v_{-\mathbf{p}+\mathbf{k}} \rangle + O(k_y/p) = \langle \eta_{\mathbf{p}} v_{-\mathbf{p}-\mathbf{k}} \rangle - \langle \eta_{\mathbf{p}-\mathbf{k}} v_{-\mathbf{p}} \rangle + O(k_y/p), \end{aligned} \quad (\text{D8})$$

and that $\langle v_{-\mathbf{p}} g_{\mathbf{p},y} \rangle = 0$ to derive Eq. (D9b). In steady state, Eqs. (D4)-(D6) lead to

$$\partial_{p_y} \left(p^4 \Re \langle vv \rangle_{\mathbf{p}\mathbf{k}} \right) = -p^4 \frac{\sqrt{2}\epsilon \chi_{\mathbf{p},y}}{p_x U'} \quad (\text{D9a})$$

$$\partial_{p_y} \left(p^2 \langle \eta v \rangle_{\mathbf{p}\mathbf{k}} \right) = ip^2 \frac{p_z}{p_x} \langle vv \rangle_{\mathbf{p}\mathbf{k}} \quad (\text{D9b})$$

$$\partial_{p_y} \Re \langle \eta \eta \rangle_{\mathbf{p}\mathbf{k}} = 2 \frac{p_z}{p_x} \Im \langle \eta v \rangle_{\mathbf{p}\mathbf{k}} - \frac{\sqrt{2}\epsilon p^2 \chi_{\mathbf{p},y}}{p_x U'}, \quad (\text{D9c})$$

after simple algebraic manipulations, and noting that $\Im(\langle vv \rangle_{\mathbf{pk}})$ and $\Im(\langle \eta\eta \rangle_{\mathbf{pk}})$ are $O(k_y/p)$.

Note that, owing to incompressibility, $u_{\mathbf{p}}$ and $w_{\mathbf{p}}$ are connected to $v_{\mathbf{p}}$ and $\eta_{\mathbf{p}}$ via

$$u_{\mathbf{p}} = -i \frac{p_z}{p_0^2} \eta_{\mathbf{p}} - \frac{p_x p_y}{p_0^2} v_{\mathbf{p}}, \quad w_{\mathbf{p}} = i \frac{p_x}{p_0^2} \eta_{\mathbf{p}} - \frac{p_y p_z}{p_0^2} v_{\mathbf{p}}, \quad (\text{D10})$$

from which we can express the Reynolds stress $\langle uv \rangle_{\mathbf{pk}}$ as a function of correlators $\langle vv \rangle_{\mathbf{pk}}$ and $\langle \eta v \rangle_{\mathbf{pk}}$:

$$\langle uv \rangle_{\mathbf{pk}} = -\frac{p_x p_y}{2(p_x^2 + p_z^2)} \langle vv \rangle_{\mathbf{pk}} + \frac{p_z}{2(p_x^2 + p_z^2)} \Im \langle \eta v \rangle_{\mathbf{pk}}. \quad (\text{D11})$$

One can further associate variables $(v_{\mathbf{p}}, \eta_{\mathbf{p}})$ to the helical variables $(a_{\mathbf{p}}^+, a_{\mathbf{p}}^-)$, via basis (A2). For the correlators, this results in applying the transform

$$\langle vv \rangle_{\mathbf{pk}} = \frac{p_0^2}{2p^2} (\Phi_{\mathbf{pk}}^+ + \Phi_{\mathbf{pk}}^-) + \Re(Z) (\Psi_{\mathbf{pk}}^{+-} + \Psi_{\mathbf{pk}}^{-+}) + i \Im(Z) (\Psi_{\mathbf{pk}}^{+-} - \Psi_{\mathbf{pk}}^{-+}) \quad (\text{D12})$$

$$\langle \eta v \rangle_{\mathbf{pk}} = p \frac{p_0^2}{2p^2} (\Phi_{\mathbf{pk}}^+ - \Phi_{\mathbf{pk}}^-) + p (Z \Psi_{\mathbf{pk}}^{+-} - Z^* \Psi_{\mathbf{pk}}^{-+}) \quad (\text{D13})$$

$$\langle \eta\eta \rangle_{\mathbf{pk}} = \frac{p_0^2}{2} (\Phi_{\mathbf{pk}}^+ + \Phi_{\mathbf{pk}}^-) - p^2 \Re(Z) (\Psi_{\mathbf{pk}}^{+-} + \Psi_{\mathbf{pk}}^{-+}) - ip^2 \Im(Z) (\Psi_{\mathbf{pk}}^{+-} - \Psi_{\mathbf{pk}}^{-+}) \quad (\text{D14})$$

to system (B16)-(B17), with $p_0^2 = p_x^2 + p_z^2$ and $Z = \frac{p_z p_y^2 - p_x^2 p^2}{2p^2 p_{\perp}^2} + i \frac{2p_x p_y p_z}{2p_{\perp}^2 p}$. With zero helicity injection, $\Psi_{\mathbf{pk}}^{+-} = \Psi_{\mathbf{pk}}^{-+*}$ and $\Phi_{\mathbf{pk}}^+ = \Phi_{\mathbf{pk}}^-$, and the transformation is simplified. Equations (D4)-(D6) can then be directly obtained from Eqs. (B16)-(B17) through this transformation (we do not detail the computation here).

Note that in the absence of cross-chirality correlations $\Psi_{\mathbf{pk}}^{+-} = 0$, and if both helicity signs are excited isotropically ($\Phi_{\mathbf{pk}}^+ = \Phi_{\mathbf{pk}}^-$), the correlation between velocity and vorticity of different waves vanishes, $\langle \eta v \rangle_{\mathbf{pk}} = 0$. As a result, velocity and vorticity are enslaved in Sector H:

$$\langle vv \rangle_{\mathbf{pk}} = \frac{p_0^2}{p^2} \Phi_{\mathbf{pk}}^s = \frac{\langle \eta\eta \rangle_{\mathbf{pk}}}{p^2}. \quad (\text{D15})$$

Appendix E: Flux coexistence due to rotation

We now consider the rotating case where the value of

$$S \equiv \frac{U'}{\Omega} \quad (\text{E1})$$

dictates which heterochiral-wave interactions with the condensate are possible. Note that the rotation rate also enters in the resonant condition for the homochiral interactions, via filter F_{k_f} (C7), but here we fix $F_{k_f} = 1$: we consider the regime where all homochiral-wave interactions contribute and do not start to decouple due to stringent resonances. This latter regime is analyzed in [30].

For fixed (p_x, p_z) , due to the resonant condition when $\tilde{s} = -s$ (B12), heterochiral interactions in Sector A emerge for $|p_y| > p_y^*$, with

$$p^*(p_z) = \frac{4|p_z|}{S} = \frac{4|p_z|\Omega}{U'}, \quad p_y^*(p_x, p_z) = \sqrt{p^{*2} - p_x^2 - p_z^2}, \quad \text{if } p^* \geq p_x^2 + p_y^2 \quad (\text{E2})$$

The surface $\Gamma = (p_x, p_y^*, p_z)$ delimiting sectors H and A is represented in Fig. 6 (orange line) in the (p_y, p_z) plane: at fixed p_z , modes $p_y < p_y^*$ are in Sector H , while modes $p_y \geq p_y^*$ are in Sector A .

Modes in Sector H have only homochiral interactions and follow the homochiral energy balance (C1). They generate a decaying small-scale energy flux (C5). Meanwhile, modes in Sector A sustain both types of interactions and obey system (D9), with boundary conditions at p_y^* imposed by the continuity of the energy flux. Sector H therefore fuels sector A. For simplicity in this section we restrict calculations to $\sigma = -\text{sgn}(U' p_x) = 1$ (i.e. $p_x < 0$) and multiply the end result by two (the direction of the p_y integration being reversed for $\sigma = -1$ but the result of the calculations being identical).

An important intersection point of the delimiting surface Γ is given by

$$p_z^1 \equiv \frac{k_f S}{4} : \quad p^*(p_z) = k_f, \quad (\text{E3})$$

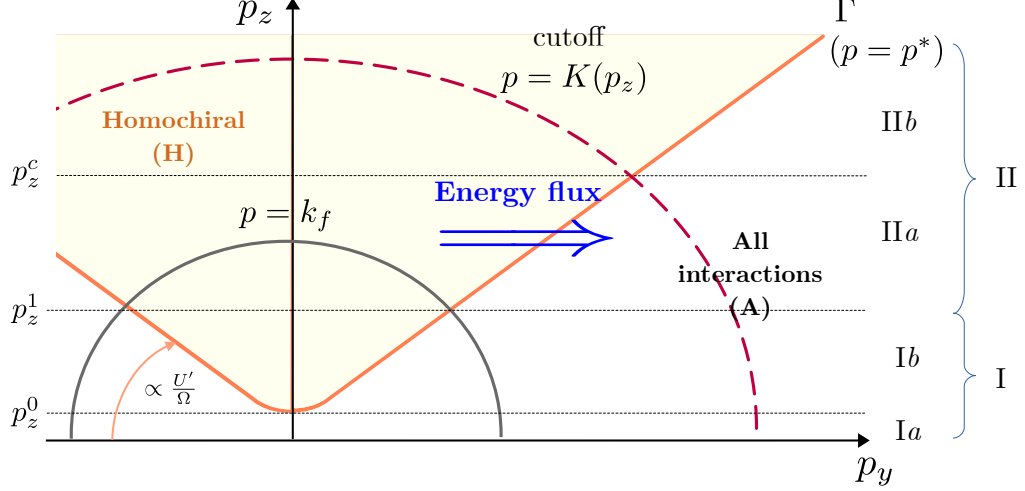


FIG. 6: Schema of the different layers in the low-rotation *mixed state*: modes in sector H (yellow zone) are only homochiral and solve Eq. (C1); modes in sector A (white zone) sustain both homochiral and heterochiral interactions and solve System (D9). The shear flow advects the energy from low to high p_y , hence from sector H to sector A. Cutoff curve $p = K$ is represented as a dashed red line (whose shape is arbitrary). Different cases emerge depending on the position of forcing and cutoff in each sector. Modes in layers Ia are all in sector A. In layers Ib, forcing occurs in A but some modes below the forcing shell are in H. In layers II (a and b), forcing occurs in H. Case IIa has $K > p^*$; Case IIb has $K < p^*$.

the p_z -value at which p_y^* meets the forcing shell $p = k_f$. Depending on the position of p_z with regard to p_z^1 , the forced modes either lie in sector *H* or in sector *A* (see Fig. 6), leading to the definitions:

- Layer II, $p_z > p_z^1$: Sector H is forced. The energy flux emerging from Sector H is transferred to Sector A.
- Layer I, $p_z < p_z^1$: Sector A is forced. Depending on the values of p_z , energy is transferred to a small part of sector H with increased p_y , before going back to sector A.

Our goal here is to derive the energy transfer from the fluctuations to the mean flow, and its leading-order behavior with variable S and domain geometry. Due to the conservation of energy, this total transfer can be computed either by integrating the Reynolds stress transfer $U' \langle uv \rangle_{\mathbf{pk}}$, or by computing the difference between the total energy flux to small scales and the energy injection rate per mode ϵ_{p_x, p_z} (assuming $F_{k_f} = 1$):

$$\begin{aligned} \frac{U'}{\sqrt{2}} \langle uv \rangle_{p_x, p_z} &\equiv \int dp_y \frac{U'}{\sqrt{2}} \langle uv \rangle_{\mathbf{pk}} \\ &= \epsilon_{p_x, p_z} - \Pi_{p_x, p_y \rightarrow \infty, p_z}, \end{aligned} \quad (\text{E4})$$

Thus, it is sufficient to compute $\Pi(p_x, p_y \rightarrow \infty, p_z)$ to obtain the total transfer of energy to the mean flow from a mode with given p_x, p_z . We will discuss the need to introduce a finite small-scale cutoff K_y in section F.

The exact computation of the spectral energy flux $\Pi_{\mathbf{p}}$ in Layers II was carried out in the End Matter (see Eq. (18)). In §E 1, we will show that the \mathbf{p} -integrated energy flux originates from these layers, producing a dominant forward energy transfer in $O\left(S \frac{L_x}{l_f}\right)$. Then, we derive the exact Reynolds stress in Layers I, and compute subleading terms coming from both Layers I and II, which we will show are in $O(S)$ and $O\left(\frac{L_x}{l_f} \sqrt{\frac{l_f}{L_z}}\right)$. These terms, in part due to discretization errors, will be included to better compare with our DNS setup.

1. Leading-order energy transfer

Layers II are forced in Sector *H*, at $p_y = \pm p_y^f$ ($p_y^f \equiv \sqrt{k_f^2 - p_x^2 - p_z^2}$), hence are solved by Eq. (C5) for $p < p^*$. As a result of single-sign-helicity conservation, the energy injected in each (p_x, p_z) line, $\epsilon_{p_x, p_z} = \frac{\epsilon F_{k_f}}{2\pi \nu p_y^f k_f}$, is transferred

to the mode p^* , with conserved helicity flux:

$$\Pi^* \equiv \Pi(p^*) = \epsilon_{p_x, p_z} \frac{k_f}{p^*}. \quad (\text{E5})$$

This flux of energy is transferred to sector A at wavenumber $p^* = \frac{4|p_z|}{S}$.

The steady-state energy flux in sector A then follows from solving system (D9), as laid out in the End Matter. Sector A is excited at $p_y = p_y^*$ and generates a small-scale energy flux

$$\Pi_{\mathbf{p}} = \frac{\Pi^*}{2} \left[1 + \frac{p^{*2}}{p^2} + \frac{p^{*2}}{p_0^2} \frac{p_z^2}{p_x^2} \left(\arctan\left(\frac{p_y}{p_0}\right) - \arctan\left(\frac{p_y^*}{p_0}\right) \right)^2 \right]. \quad (\text{E6})$$

The \mathbf{p} -dependent Reynolds transfer associated to Layers II is:

$$\frac{U'}{\sqrt{2}} \langle uv \rangle_{\mathbf{p}\mathbf{k}} = \sqrt{2} U' \left(-\frac{p_x p_y}{p_0^2} \langle v v \rangle_{\mathbf{p}\mathbf{k}} + \frac{p_z}{p_0^2} \Im \langle \eta v \rangle_{\mathbf{p}\mathbf{k}} \right) \quad (\text{E7})$$

$$= \begin{cases} k_f \epsilon_{p_x, p_z} \frac{p_y}{2p^3}, & -p_y^f < p_y < p_y^f \\ k_f \epsilon_{p_x, p_z} \frac{p_y}{p^3}, & p_y^f < p_y < p_y^* \\ k_f \epsilon_{p_x, p_z} \left[\frac{p^* p_y}{p^4} - \frac{p_z^2 p^*}{p_x^2 p_0} \frac{1}{p^2} \left(\arctan\left(\frac{p_y}{p_0}\right) - \arctan\left(\frac{p_y^*}{p_0}\right) \right) \right], & p_y > p_y^* \end{cases} \quad (\text{E8})$$

With zero helicity injection, and if all homochiral-wave interactions are resonant ($F_{k_f} = 1$), the total energy balance between the small-scale flux $\Pi_{\mathbf{p}}$ (E6) and the transfer to the mean flow from layers II is therefore:

$$\frac{U'}{\sqrt{2}} \langle uv \rangle_{p_x, p_z}^{\text{II}} \equiv \int dp_y \frac{U'}{\sqrt{2}} \langle uv \rangle_{\mathbf{p}\mathbf{k}}^{\text{II}} = \epsilon_{p_x, p_z} - \Pi_{p_x, K_y, p_z}, \quad (\text{E9})$$

with K_y a given wavenumber cutoff. In the limit $K_y \rightarrow \infty$, we therefore obtain the leading-order energy transfer due to the (p_x, p_z) layer:

$$\frac{U'}{\sqrt{2}} \langle uv \rangle_{p_x, p_z}^{\text{II}} = \epsilon_{p_x, p_z} \left[\underbrace{1}_{\text{energy input from H}} - \underbrace{\frac{k_f}{2p^*} - \frac{p_z^2}{p_x^2} \frac{k_f p^*}{2p_0^2} \left(\frac{\pi}{2} - \arctan\left(\frac{p_y^*}{p_0}\right) \right)^2}_{\text{energy extraction from A}} \right] \quad (\text{E10})$$

We now extract the leading order functional form of the Reynolds stress in the variable $S = \frac{U'}{\Omega}$. Here we consider that S is sufficiently large ($S \gtrsim l_f/L_y$, following the computation in [30]) so that all the waves excited at the forcing scale are coupled with the condensate via homochiral interactions, hence $F_{k_f} = 1$. We also assume that

$$\frac{S}{4} \ll 1 \Rightarrow \frac{p^*}{p_0} = 4 \frac{|p_z|}{S p_0} \gg 1 \quad (\text{E11})$$

while keeping $S = O(1)$. We will find that $S \lesssim 1$ so that $S/4 \lesssim 0.25$ and this approximation holds. The selection of large $|p_z|$ when $S/4 \ll 1$ is consistent with Layers II having $p^* = 4|p_z|/S > k_f > p_0$. Therefore, wavenumber $p_y^* = \sqrt{p^{*2} - p_0^2} \approx p^* = \frac{4|p_z|}{S}$ at the leading order in $S/4$. Hence, under the approximation (E11), $p_y^*/p_0 \gg 1$ and we can approximate $\frac{\pi}{2} - \arctan\left(\frac{p_y^*}{p_0}\right) \approx \frac{p_0}{p_y^*} \approx \frac{S p_0}{4|p_z|}$ in (E10) and obtain:

$$\frac{U'}{\sqrt{2}} \langle uv \rangle_{p_x, p_z}^{\text{II}} \approx \frac{\epsilon}{2\pi k_f \sqrt{k_f^2 - p_x^2 - p_z^2}} \left[1 - \frac{S k_f}{8|p_z|} \left(1 + \frac{p_z^2}{p_x^2} \right) + O\left(\left(\frac{S}{4} \right)^3 \frac{k_f p_0^2}{p_z p_x^2} \right) \right] \quad (\text{E12})$$

Note that modes $p_z \sim p_z^1 = k_f S/4$ are not very far from $p_0 S/4$ and can break the separation (E11), but we still expect (E12) to yield a good leading order estimate. Indeed, $\arctan\left(\frac{p_y^*}{p_0}\right)$ is generally close to $\frac{\pi}{2} - \frac{p_0}{p_y^*}$ when $p_y^* > p_0$, even when $p_y^* \gg p_0$ does not strictly hold. In the following, we drop the correction term in (E12).

The total energy transfer from layers II is obtained by integrating modes with $p_z \geq Sk_f/4$, hence considering $-k_f\sqrt{1 - (\frac{S}{4})^2} \leq p_x \leq -\frac{2\pi}{L_x}$. From Eq. (E12), we can anticipate that the term in p_z/p_x^2 will give the leading-order contribution of the production of kinetic energy when it is the largest possible, i.e. of the order of L_x^2/l_f^2 . In particular, this term will dominate the second term in $k_f/|p_x|$. This term being not-integrable around $p_x \rightarrow 0$, we need to cutoff the integration over p_x at $p_x = 2\pi/L_x$.

When first integrating over p_z , we use the integrals

$$\int dp_z \frac{1}{\sqrt{k_f^2 - p_x^2 - p_z^2}} = \arctan\left(\frac{p_z}{\sqrt{k_f^2 - p_x^2 - p_z^2}}\right), \quad (\text{E13})$$

$$\int dp_z \frac{1}{p_z \sqrt{k_f^2 - p_x^2 - p_z^2}} = \frac{1}{2\sqrt{k_f^2 - p_x^2}} \left(\log\left(\sqrt{k_f^2 - p_x^2} + \sqrt{k_f^2 - p_x^2 - p_z^2}\right) - \log\left(\sqrt{k_f^2 - p_x^2} - \sqrt{k_f^2 - p_x^2 - p_z^2}\right) \right), \quad (\text{E14})$$

$$\int dp_z \frac{p_z}{\sqrt{k_f^2 - p_x^2 - p_z^2}} = \sqrt{k_f^2 - p_x^2 - p_z^2}, \quad (\text{E15})$$

to obtain that

$$\begin{aligned} T_{3\text{D}-2\text{D}}^{\text{II}} &= \frac{4\mathcal{V}}{\sqrt{2}} \int_{-\frac{2\pi}{L_x}}^{-\frac{2\pi}{L_x}} \int_{-\sqrt{k_f^2 - (\frac{Sk_f}{4})^2}}^{\sqrt{k_f^2 - p_x^2}} \int_{\frac{Sk_f}{4}}^{Sk_f} U' \langle uv \rangle_{p_x, p_z}^{\text{II}} dp_z dp_x \quad (\text{E16}) \\ &= \frac{2\epsilon}{\pi} \int_{\frac{2\pi}{L_x}}^{\sqrt{k_f^2 - (\frac{Sk_f}{4})^2}} \left\{ \frac{1}{k_f} \left(\frac{\pi}{2} - \arctan\left(\frac{Sk_f}{4\sqrt{k_f^2 - p_x^2 - (\frac{k_f S}{4})^2}}\right) \right) \right. \\ &\quad \left. - \frac{S}{8} \left[\frac{1}{2\sqrt{k_f^2 - p_x^2}} \left(\log\left(\sqrt{k_f^2 - p_x^2} + \sqrt{k_f^2 - p_x^2 - (\frac{Sk_f}{4})^2}\right) - \log\left(\sqrt{k_f^2 - p_x^2} - \sqrt{k_f^2 - p_x^2 - (\frac{Sk_f}{4})^2}\right) \right) \right. \right. \\ &\quad \left. \left. + \frac{1}{p_x^2} \sqrt{k_f^2 - p_x^2 - \frac{S^2 k_f^2}{16}} \right] \right\} dp_x + \mathcal{C}_{\text{disc}, p_z}, \quad (\text{E17}) \end{aligned}$$

with corrections $\mathcal{C}_{\text{disc}, p_z} \ll \epsilon$ due to discretization errors arising when treating p_z as a continuous variable. Recall that we consider a periodic system of finite size, therefore our development concerns the evaluation of discrete sums, which we approximate as continuous integrals.

Equation (E17) can now be simplified with further expanding in $S/4 \ll 1$:

$$\begin{aligned} \frac{T_{3\text{D}-2\text{D}}^{\text{II}}}{\epsilon} &\approx \frac{2}{\pi} \int_{\frac{2\pi}{L_x}}^{\sqrt{k_f^2 - (\frac{Sk_f}{4})^2}} dp_x \left[\underbrace{\frac{1}{k_f} \frac{\pi}{2} - \frac{S}{4} \frac{1}{\sqrt{k_f^2 - p_x^2}}}_{\mathcal{I}, \text{ energy input from H}} - \underbrace{\frac{S}{8} \frac{\log\left(\frac{2\sqrt{k_f^2 - p_x^2}}{Sk_f/4}\right)}{\sqrt{k_f^2 - p_x^2}} - \frac{S}{8} \frac{1}{p_x^2} \sqrt{k_f^2 - p_x^2}}_{\mathcal{D}, \text{ energy extraction from A}} \right] \\ &\quad + O\left(\frac{L_x}{l_f} \left(\frac{S}{4}\right)^3\right) + \mathcal{C}_{\text{disc}, p_z} \quad (\text{E18}) \end{aligned}$$

with corrections in $O(L_x(S/4)^3)$ arising due to the expansion in $S/4$. In the following we estimate each term in (E18) individually.

We start with the leading-order term in L_x/l_f , which comes from the last term in the integral in (E18). This term is not integrable at $p_x = 0$, and its p_x -integral must therefore be interpreted carefully. With finite size L_x , our development actually concerns a discrete sum in (E18), whose lower bound is the same as the step $dp_x = 2\pi/L_x$. We therefore want to estimate

$$r_x \sum_{\substack{p_x = m r_x, m \in \mathbb{N} \\ r_x \leq p_x \leq \sqrt{k_f^2 - (\frac{Sk_f}{4})^2}}} \frac{1}{p_x^2} \sqrt{k_f^2 - p_x^2}, \quad (\text{E19})$$

with $r_x \equiv 2\pi/L_x$ being both the grid spacing and a cutoff at the first grid point. If the lower bound in the sum was fixed (e.g. $p_x = 1$), we would use the Riemann result to obtain an integral of the continuous variable $p_x \in \mathbb{R}$, which yields a good estimate of the sum. However, here the lower bound evolves with the discretization parameter. A corrected estimate can be obtained by the Euler-Maclaurin series

$$\sum_{p_x=r_x}^{\sqrt{k_f^2 - \left(\frac{Sk_f}{4}\right)^2}} \frac{1}{p_x^2} \sqrt{k_f^2 - p_x^2} = \frac{1}{r_x} \int_{r_x}^{k_f} f(p_x) + \frac{f\left(\sqrt{k_f^2 - \left(\frac{Sk_f}{4}\right)^2}\right) + f(r_x)}{2} + \frac{r_x}{24} \left[f'\left(\sqrt{k_f^2 - \left(\frac{Sk_f}{4}\right)^2}\right) - f'(r_x) \right] \quad (\text{E20})$$

denoting $f(p_x) = \sqrt{k_f^2 - p_x^2}/p_x^2$ a function of the continuous variable $p_x \in [k_x, k_f]$. Here we have truncated the Euler-Maclaurin series at the second order, assuming the next orders be small due to their diminishing prefactors. However, these next order terms are not necessarily small in the parameter $r_x/k_f = l_f/L_x$. More explicitly, using that $\int dp_x \frac{1}{p_x^2} \sqrt{k_f^2 - p_x^2} = -\frac{\sqrt{k_f^2 - p_x^2}}{p_x} - \arctan\left(\frac{p_x}{\sqrt{k_f^2 - p_x^2}}\right)$, this leads to

$$\begin{aligned} \sum_{p_x=r_x}^{\sqrt{k_f^2 - \left(\frac{Sk_f}{4}\right)^2}} \frac{1}{p_x^2} \sqrt{k_f^2 - p_x^2} &= \frac{1}{r_x} \left[\frac{\sqrt{k_f^2 - r_x^2}}{r_x} + \arctan\left(\frac{r_x}{\sqrt{k_f^2 - r_x^2}}\right) - \frac{\pi}{2} + O\left(\frac{S}{4}\right)^3 \right] + \frac{1}{2r_x^2} \sqrt{k_f^2 - r_x^2} \\ &+ \frac{r_x}{24} \left[f'\left(\sqrt{k_f^2 - \left(\frac{Sk_f}{4}\right)^2}\right) + \frac{1}{r_x \sqrt{k_f^2 - r_x^2}} + \frac{2}{r_x^3} \sqrt{k_f^2 - r_x^2} \right]. \end{aligned} \quad (\text{E21})$$

The problem raised by estimating the sum with only the integral can be appreciated as $f(r_x) \sim 1/r_x^2$ leads to a term of the same order as the integral. Note that $f'\left(\sqrt{k_f^2 - \left(\frac{Sk_f}{4}\right)^2}\right) \simeq \frac{4}{Sk_f^2} + \frac{S}{2k_f^2}$ so that its contribution is negligible compared to $2k_f/r_x^3$ when $r_x/k_f \rightarrow 0$ (also recall that this term is multiplied by $S/4$ in equation (E12)).

All in all, we obtain the leading order asymptotics

$$r_x \sum_{p_x=r_x}^{\sqrt{k_f^2 - \left(\frac{Sk_f}{4}\right)^2}} \frac{1}{p_x^2} \sqrt{k_f^2 - p_x^2} = \frac{19}{12} \frac{L_x}{l_f} - \frac{\pi}{2} + O\left(\frac{l_f}{L_x}\right) + O\left(\left(\frac{L_x S}{l_f}\right)^3\right) \quad (\text{E22})$$

with $l_f = 2\pi/k_f$.

All terms in (E18) other than the last one can be estimated with their continuous integrals at the leading order.

For the third term in (E18), we use that

$$\int_0^1 \frac{\log(2\sqrt{1-x^2})}{\sqrt{1-x^2}} = 0 \quad (\text{E23})$$

so that

$$\frac{2\epsilon}{\pi} \int_{\frac{2\pi}{L_x}}^{\sqrt{k_f^2 - \left(\frac{Sk_f}{4}\right)^2}} \frac{S \log\left(\frac{2\sqrt{k_f^2 - p_x^2}}{Sk_f/4}\right)}{\sqrt{k_f^2 - p_x^2}} = -\frac{S}{8} \log \frac{S}{4} + O\left(\frac{l_f}{L_x}\right) + O\left(\left(\frac{S}{4}\right)^{\frac{3}{2}} \log \frac{S}{4}\right) \quad (\text{E24})$$

where the last term comes from the upper bound of the integral, $\int_{1-\epsilon}^1 \frac{\log(2\sqrt{1-x^2})}{\sqrt{1-x^2}} \simeq \int_0^\epsilon \frac{\log \sqrt{2u}}{\sqrt{2u}} \simeq -\sqrt{\frac{\epsilon}{2}} \log \epsilon$, with $\epsilon = S/4$. Deviations from the discrete sum are here also in $O\left(\sqrt{\frac{l_f}{L_x}}\right)$.

For the energy input term in (E18), using that $\int dp_x \frac{1}{\sqrt{k_f^2 - p_x^2}} = \arctan\left(\frac{p_x}{\sqrt{k_f^2 - p_x^2}}\right)$, we obtain that

$$\frac{\mathcal{I}}{\epsilon} = \frac{2}{\pi} r_x \sum \left(1 - \frac{S}{4} \frac{1}{\sqrt{k_f^2 - p_x^2}} \right) = 1 - \frac{S}{4} + O\left(\frac{S}{4} \sqrt{\frac{l_f}{L_x}}\right) + O\left(\frac{l_f}{L_x}\right) \quad (\text{E25})$$

using the Mac Laurin expansion for the correction term due to discretization errors in p_x , coming from the term in $S/4$.

We finally obtain at the leading order in L_x/l_f and $S/4$:

$$\frac{T_{3D-2D}^{\text{II}}}{\epsilon} = \mathcal{I} - \mathcal{D} \quad (\text{E26})$$

$$\approx 1 - \frac{S}{4} \left(\frac{19}{12} \frac{L_x}{\pi l_f} + \frac{1}{2} - \frac{1}{2} \log \frac{S}{4} \right) \quad (\text{E27})$$

$$\approx 1 - \frac{S}{4} \frac{19}{12\pi} \frac{L_x}{l_f} + O\left(\frac{S}{4}\right), \quad S = \frac{U'}{\Omega}, \quad (\text{E28})$$

Note here that we have considered that the term $S/4 \log S/4$, which produces a steeper-than-linear behavior when $S \rightarrow 0$, is bounded by $O(S/4)$ when $S/4 \ll 1$. Corrections to (E28) other than those determined so far might involve combinations of functions of S and $L_x/l_f, L_z/l_f$, which we determine in §E3.

The energy transfer between the waves and the 2D condensate in (E28) decreases with decreasing rotation, via increasing $S = U'/\Omega$, due to the growing number of modes in sector A that break conservation of $H_{\mathbf{p}}^{\pm}$ and extract mean-flow energy. This energy extraction is larger as L_x/l_f increases, due to vortex-tilting preferentially energizing modes with large $p_z/p_x \sim L_x/l_f$, via the term in p_z/p_x in (E10).

The energy extraction in Layers I should follow the same logic in terms of L_x/l_f dependence, with a production of kinetic energy at small scales in p_z^2/p_x^2 , similarly to that in Layers II (Eq. (E10)). However, as Layers I are constrained by $p_z < Sk_f/4 \ll k_f$, there are fewer modes in Layers I within our approximation (E11), so the production of kinetic energy should be bounded by $p_z^2/p_x^2 \sim (S/4)^2/p_x^2$, hence an order $(S/4)^2$ lower than that in layers II, and to the left-most term in Eq. (18). Therefore, we expect Layers I to dominantly behave as 2D-3C modes $p_z = 0$, transferring energy to small scales at rate $\Pi^I \sim \epsilon_{p_x, p_z}/2$ at leading order in S . (The factor 1/2 comes from the vertical component w producing small-scale energy.)

These qualitative arguments on Layers I will be confirmed in §E2 and E3b, where we compute the energy flux due to these layers, and confirm it is of subleading order compared to (E28). We will also detail why layers I can be fully neglected compared to layers II with the parameter choice in our DNS ($L_x k_f = 5$), even at $O(S/4)$.

2. Exact energy transfer

In the following, we compute all the contributions to the Reynolds stress, including Layers I. We also introduce an arbitrary cutoff $K(p_z)$ over which the Reynolds stress is integrated. Modes $p > K$ supposedly do not contribute to the Reynolds stress, due to the dominance of other interaction types (eddy-eddy or wave-wave) that break the QL assumption. Introducing such a cutoff has a particular physical importance at low rotation, which we discuss in §F.

We further introduce two intersection points of the surface Γ . First,

$$p_z^0 \equiv \frac{|p_x|}{(\frac{16}{S^2} - 1)^{1/2}} : \quad p_y^*(p_x, p_z^0) = 0, \quad (\text{E29})$$

is the p_z value where Γ crosses the plane $p_y = 0$. Then, for a given p_x and for $p_z < p_z^0(p_x)$ we define $p_y^* \equiv 0$. Second,

$$p_z^c = \frac{SK}{4} \quad (\text{E30})$$

is the value of p_z at which the cutoff-curve $K(p_z)$ intersects Γ (see Fig. 6).

For modes in layers I, the geometry of the curve Γ imposes two possible sub-cases:

Ia – The p_z -layer is below the parabola Γ ($|p_z| < p_z^0$ and $p_y^* = 0$): all modes are in sector A ;

Ib – Sector A is forced, but a parabolic section below the forcing shell lies in Sector H ($p_z^1 > |p_z| > p_z^0$). With increased p_y , energy is transferred to Sector H when $p_y > -p_y^*$, and back to Sector A when $p_y > p_y^*$.

Note that introducing a cutoff at K also leads to two further distinctions in layers II:

– Layers IIa – ($p_z > p_z^c$) The energy flux emerging from Sector H is transferred to Sector A, and is eventually cutoff. This case is solved by (E6), cut-off at K .

– Layers IIb – ($p_z < p_z^c$) The energy flux emerging from Sector H is cutoff before it can enter sector A ($K < p^*$). This case is solved by (C5), cut-off at K .

We now detail the computation of the Reynolds stresses in layers Ib (see Fig. 6), from which Layers Ib follow (by setting $p_y^* = 0$). There, all stresses are integrated from $p_y = -p_y^f \equiv -\sqrt{k_f^2 - p_x^2 - p_z^2}$ to $p_y = K_y = \sqrt{K^2 - p_0^2}$, the p_y mode corresponding to a given cutoff K . As we did for the leading-order transfer in E1, we only focus on increasing p_y and $p_x < 0$, the other relevant quadrant being obtained by taking $p_x \rightarrow -p_x$ and $p_y \rightarrow -p_y$ (recall that quadrants $p_x p_y > 0$ are not energized by the shear-flow advection).

a. Reynolds stress in Layers I

In the p_z -layers such that $p_z^0 < |p_z| < p_z^1$ (Layers Ia in 6), modes are forced in Sector A, then enter Sector H (for $p_y \in [-p_y^*, p_y^*]$), before going back to Sector A (for $p_y > p_y^*$).

Modes $p_y < -p_y^*$, by construct in Sector A, receive an energy flux $\epsilon_{p_x, p_z}/2$ from the forcing shell at $-p_y^f$. The corresponding velocity and vorticity correlators for $-p_y^f < p_y < -p_y^*$ are therefore

$$\begin{aligned} \langle vv \rangle_{\mathbf{pk}} &= \frac{\epsilon_{p_x, p_z}}{2\sqrt{2}p_x U'} \frac{p_0^2 k_f^2}{p^4}, \\ \langle \eta v \rangle_{\mathbf{pk}} &= i \frac{\epsilon_{p_x, p_z}}{2\sqrt{2}p_x U'} p_0 \frac{p_z}{p_x} \frac{k_f^2}{p^2} \left[\arctan\left(\frac{p_y}{p_0}\right) + \arctan\left(\frac{p_y^f}{p_0}\right) \right], \quad -p_y^f < p_y < -p_y^* \end{aligned} \quad (\text{E31})$$

with $\epsilon_{p_x, p_z} = \frac{\epsilon F k_f}{2\pi \nu p_y^f k_f}$.

Modes $-p_y^* < p_y < p_y^*$ are in Sector H, hence conserve their sign-definite helicity

$$\Phi_{\mathbf{pk}}^s = \frac{\epsilon_{p_x, p_z}}{2p_x U'} \frac{k_f^2}{p^* p}, \quad (\text{E32})$$

using the continuity of the flux at $-p_y^*$, $\Phi_{\mathbf{pk}}^s = \frac{p^{*2}}{p_0^2} \langle vv \rangle_{\mathbf{pk}}(-p_y^*)$. Because Eq. (C1) exhibits $p_y \rightarrow -p_y$ symmetry, the boundary condition at $-p_y^*$ dictates the values of the correlators at p_y^* .

For $p_y > p_y^*$, modes are in Sector A, and follow Eq. (D9) with forcing at $p_y = p_y^f$:

$$\langle vv \rangle_{\mathbf{pk}} = \langle vv \rangle_{\mathbf{pk}}(-p_y^*) \frac{p^{*4}}{p^4} + \frac{\sqrt{2}\epsilon}{2|U' p_x| p^4} \int_{p_y^*}^{p_y} q^4 \left(1 - \frac{q_y^2}{q^2}\right) \chi_q dq_y = \begin{cases} \frac{\epsilon_{p_x, p_z}}{2\sqrt{2}|U' p_x|} \frac{p_0^2 k_f^2}{p^4}, & p_y^* < p_y < p_y^f \\ \frac{\epsilon_{p_x, p_z}}{\sqrt{2}|U' p_x|} \frac{p_0^2 k_f^2}{p^4}, & p_y > p_y^f \end{cases} \quad (\text{E33})$$

$$\langle \eta v \rangle_{\mathbf{pk}} = \langle \eta v \rangle_{\mathbf{pk}}(-p_y^*) \frac{p^{*2}}{p^2} + \frac{i}{p^2} \int_{p_y^*}^{p_y} \frac{p_z}{p_x} q^2 v_q^2 dq_y = \begin{cases} i \frac{\epsilon_{p_x, p_z} p_0}{2\sqrt{2}U' p_x} \frac{p_z}{p_x} \frac{k_f^2}{p^2} \left[\arctan\left(\frac{p_y}{p_0}\right) + \arctan\left(\frac{p_y^f}{p_0}\right) - 2 \arctan\left(\frac{p_y^*}{p_0}\right) \right], & p_y^* < p_y < p_y^f \\ i \frac{\epsilon_{p_x, p_z} p_0}{\sqrt{2}U' p_x p_y^f} \frac{p_z}{p_x} \frac{k_f^2}{p^2} \left[\arctan\left(\frac{p_y}{p_0}\right) - \arctan\left(\frac{p_y^*}{p_0}\right) \right], & p_y > p_y^f \end{cases}$$

Overall, this leads to the Reynolds stress in layers Ib:

$$\langle uv \rangle_{\mathbf{pk}} = \begin{cases} \frac{\epsilon_{p_x, p_z} k_f^2}{\sqrt{2}U'} \left[\frac{p_y}{p^4} - \frac{p_z^2}{p_x^2} \frac{1}{p_0} \frac{1}{p^2} \left(\arctan\left(\frac{p_y}{p_0}\right) + \arctan\left(\frac{p_y^f}{p_0}\right) \right) \right], & -p_y^f < p_y < -p_y^* \\ \frac{\epsilon_{p_x, p_z} k_f^2}{\sqrt{2}U'} \left[\frac{p_y}{p^4} - \frac{p_z^2}{p_x^2} \frac{1}{p_0} \frac{1}{p^2} \left(\arctan\left(\frac{p_y}{p_0}\right) + \arctan\left(\frac{p_y^f}{p_0}\right) - 2 \arctan\left(\frac{p_y^*}{p_0}\right) \right) \right], & p_y^* < p_y < p_y^f \\ \frac{\sqrt{2}\epsilon_{p_x, p_z} k_f^2}{U'} \left[\frac{p_y}{p^4} - \frac{p_z^2}{p_x^2} \frac{1}{p_0} \frac{1}{p^2} \left(\arctan\left(\frac{p_y}{p_0}\right) - \arctan\left(\frac{p_y^*}{p_0}\right) \right) \right], & p_y > p_y^f \end{cases} \quad (\text{E34})$$

In Fig. 1e in the main text, we visualize $U'\langle uv \rangle_{\mathbf{pk}}$ in the (p_y, p_z) plane by showing Eq. (E34) in layers I, completing the Reynolds stress in layers II (Eq. (E8)). In the figure, we fix $p_x = 8\pi/L_x$ and $S = 1$.

From Eq. (E34), the p_y -integrated Reynolds stress is

$$\langle uv \rangle_{p_x, p_z}^I = \frac{\sqrt{2}\epsilon_{p_x, p_z} k_f^2}{2U'} \left[\left(\frac{1}{k_f^2} - \frac{1}{K^2} \right) - \frac{p_z^2}{p_x^2} \frac{1}{p_0^2} \left[\left(\arctan\left(\frac{K_y}{p_0}\right) - \arctan\left(\frac{p_y^*}{p_0}\right) \right)^2 + \left(\arctan\left(\frac{p_y^f}{p_0}\right) - \arctan\left(\frac{p_y^*}{p_0}\right) \right)^2 \right] \right] \quad (\text{E35})$$

Case Ia, where sector H is not crossed and modes lie entirely in sector A, is included in Eq. (E35) by setting $p_y^* = 0$. This case corresponds to a non-rotating shear flow, as layers Ia are fully unconstrained by rotation.

b. Summary of the exact Reynolds stress

The exact total transfer obtained from our computation of the different p_z -layers is finally written as

$$\frac{T_{3D-2D}}{\epsilon} = \frac{4U'\mathcal{V}}{\sqrt{2}\epsilon} \int_{-k_f}^{-\frac{2\pi}{L_x}} dp_x \left(\int_{\frac{2\pi}{L_x}}^{\frac{k_f S}{4}} \langle uv \rangle_{p_x, p_z}^I dp_z + \int_{\frac{k_f S}{4}}^{\sqrt{k_f^2 - p_x^2}} \langle uv \rangle_{p_x, p_z}^{\text{II}} dp_z \right), \quad (\text{E36})$$

$$\langle uv \rangle_{p_x, p_z}^I = \frac{\sqrt{2}\epsilon_{p_x, p_z}}{2U'} \left[\left(1 - \frac{k_f^2}{K^2} \right) - \frac{p_z^2}{p_x^2} \frac{k_f^2}{p_0^2} \left[\left(\arctan\left(\frac{K_y}{p_0}\right) - \arctan\left(\frac{p_y^*}{p_0}\right) \right)^2 + \left(\arctan\left(\frac{p_y^f}{p_0}\right) - \arctan\left(\frac{p_y^*}{p_0}\right) \right)^2 \right] \right] \quad [\text{Layers I, } K = \min(k_U^{\text{wave}}, k_U^{\text{eddy}})] \quad (\text{E37})$$

$$\langle uv \rangle_{p_x, p_z}^{\text{II}} = \begin{cases} \frac{\sqrt{2}\epsilon_{p_x, p_z}}{U'} \left[1 - \frac{k_f}{2p^*} \left(1 + \frac{p^{*2}}{K^2} + \frac{p_z^2}{p_x^2} \frac{p^{*2}}{p_0^2} \left(\arctan\left(\frac{K_y}{p_0}\right) - \arctan\left(\frac{p_y^*}{p_0}\right) \right)^2 \right) \right] & \text{if } p_z < \frac{SK}{4} \\ \frac{\sqrt{2}\epsilon_{p_x, p_z}}{U'} \left[1 - \frac{k_f}{K} \right] & \text{if } p_z \geq \frac{SK}{4} \quad [\text{Layers IIa, } K = \min(k_U^{w.t}, k_U^{\text{eddy}})] \\ \frac{\sqrt{2}\epsilon_{p_x, p_z}}{U'} \left[1 - \frac{k_f}{K} \right] & \text{if } p_z \geq \frac{SK}{4} \quad [\text{Layers IIb, } K = \min(k_\Omega, k_U^{\text{wave}})] \end{cases} \quad (\text{E38})$$

with $p^* = 4|p_z|/S$, $p_y^* = (p^{*2} - p_0^2)^{1/2}$, $p_0^2 = p_x^2 + p_z^2$, $K_y = (K^2 - p_0^2)^{1/2}$

where $S \equiv \frac{U'}{\Omega}$, K is an arbitrary cutoff depending on p_z , Ω and U' , and ϵ_{p_x, p_z} the energy injection rate in each line (p_x, p_z) . We will elaborate on the definition of cutoffs $K = k_\Omega, k_U^{\text{wave}}$ or k_U^{eddy} in §F (Eqs. (F4)-(F6)), but write them here for consistency. In this current section §E, we only discuss the non-cutoff case $K \rightarrow \infty$.

3. Subleading corrections to the energy transfer

We now derive subleading corrections to solution (E28). These corrections will perfect the agreement with our DNS data and are also important for consistency and completeness. In particular, we will establish why (E28) is the correct estimate for the *total* energy transfer between the waves and the condensate, hence why Layers I only contribute to subleading order.

a. Layers II

First, note that we willingly dropped the term in $O\left(\left(\frac{S}{4}\right)^3 \frac{k_f(p_x^2 + p_z^2)}{p_x p_z^2}\right)$ in Eq. (E12), coming from the expansion in $S/4 \ll 1$. Over integration, this term generates a correction to the total energy transfer in $\left(\frac{S}{4}\right)^3 \left[\log\left(\frac{S}{4}\right) + L_x k_f \right] = O\left(\left(\frac{S}{4}\right)^3 L_x k_f\right)$, which is of the same order than the correction in Eq. (E18).

The important source of corrections now arises due to discretization errors, in particular those due to the p_z -integration, denoted by $\mathcal{C}_{\text{disc}, p_z}$ in (E18). These can be estimated via the Euler-Maclaurin formula as follows (we

denote $r_z = 2\pi/L_z$ and $\alpha = \sqrt{k_f^2 - p_x^2}$:

$$\mathcal{C}_{\text{disc}, p_z} = \frac{r_z}{2} \left((\text{E12})|_{p_z=\alpha-r_z} + (\text{E12})|_{p_z=\frac{Sk_f}{4}} \right) \quad (\text{E39})$$

$$\simeq \frac{\epsilon}{\pi} \frac{r_z}{k_f} \int_{\frac{2\pi}{L_x}}^{k_f} dp_x \frac{1}{\sqrt{2r_z\alpha}} \left[1 - \frac{Sk_f}{8\alpha} \left(1 + \frac{\alpha^2}{p_x^2} \right) \right] + \frac{\epsilon}{\pi} \frac{r_z}{k_f} \int_{\frac{2\pi}{L_x}}^{k_f} dp_x \frac{1}{\sqrt{\alpha^2 - (\frac{Sk_f}{4})^2}} \left[1 - \frac{1}{2} \left(1 + \frac{1}{p_x^2} \left(\frac{Sk_f}{4} \right)^2 \right) \right] \quad (\text{E40})$$

$$\approx \frac{\epsilon}{\pi} \frac{r_z}{k_f} \int_{\frac{2\pi}{L_x}}^{k_f} dp_x \frac{1}{\sqrt{2r_z k_f}} \left[1 - \frac{S}{8} \left(1 + \frac{k_f^2}{p_x^2} \right) \right] + \frac{\epsilon}{\pi} \frac{r_z}{k_f} \int_{\frac{2\pi}{L_x}}^{k_f} dp_x \frac{1}{\alpha} \left[1 - \frac{1}{2p_x^2} \left(\frac{Sk_f}{4} \right)^2 \right], \quad (\text{E41})$$

when considering only modes $p_x \ll k_f$ in the first sum, which give the dominant contribution in $L_x k_f$:

$$\mathcal{C}_{\text{disc}, p_z} \approx \frac{\epsilon}{\pi} \sqrt{\frac{l_f}{2L_z}} \left[1 - \frac{S L_x}{8 l_f} \right] + O\left(\frac{l_f}{L_z} \frac{L_x}{l_f}\right) = O\left(\frac{S L_x}{4 l_f} \sqrt{\frac{l_f}{L_z}}\right) \quad (\text{E42})$$

Note that we exclude the thin layer case $L_x k_f \sim 1$ in this paper, where our p_z -integration does not hold. However, a situation where $L_x \gg L_z$ could arise where this term is relevant. Furthermore, with our parameter choice, these terms are not negligible compared to $O\left(\frac{S}{4}\right)$.

The leading-order discretization errors due to the p_x -integrations are already included in solution (E28), as they contribute at $O\left(\frac{S L_x}{4 l_f}\right)$. Other discretization errors, due to the p_x -integrable terms in (E18), are in $O(S\sqrt{L_x/l_f})$, like the one arising in (E25).

All in all we obtain the corrected energy transfer in layers II:

$$T_{3\text{D}-2\text{D}}^{\text{II}} = \epsilon' \left[1 + \frac{1}{\pi} \sqrt{\frac{l_f}{2L_z}} - \frac{S}{4} \left(\frac{19 L_x}{12 \pi l_f} + \frac{1}{2} - \frac{1}{2} \log \frac{S}{4} - \frac{1}{2\pi} \frac{L_x}{l_f} \sqrt{\frac{l_f}{2L_z}} \right) \right. \\ \left. + O\left(\sqrt{\frac{l_f}{L_x}}\right) + O\left(\frac{l_f}{L_x}\right) + O\left(\frac{L_x}{l_f} \left(\frac{S}{4}\right)^3\right) + O\left(\left(\frac{S}{4}\right)^{\frac{3}{2}} \log \frac{S}{4}\right) \right] \quad (\text{E43})$$

with $\epsilon' = \epsilon / \left(1 + \frac{1}{\pi} \sqrt{\frac{l_f}{2L_z}}\right)$ the energy injection rate corrected to include discretization errors.

b. Layers I

The energy transfer in layers I (E35) is written as

$$\frac{U'}{\sqrt{2}} \langle uv \rangle_{p_x, p_z}^{\text{I}} = \frac{\epsilon_{p_x, p_z}}{2} \left[\underbrace{\mathcal{I}}_{\text{input from H}} \underbrace{- \frac{p_z^2 k_f^2}{p_x^2 p_0^2} \left[\left(\frac{\pi}{2} - \arctan\left(\frac{p_y^*}{p_0}\right) \right)^2 + \left(\arctan\left(\frac{p_y^f}{p_0}\right) - \arctan\left(\frac{p_y^*}{p_0}\right) \right)^2 \right]}_{\mathcal{D}, \text{extraction from A}} \right] \quad (\text{E44})$$

when $K \rightarrow \infty$. Note here the prefactor 1/2, which governs the injection of energy for $p_z \rightarrow 0$: quasi-2D layers conserve horizontal enstrophy, and exhibit a forward cascade of the vertical component w , which produces small-scale energy. Energy is therefore equally distributed in the two dynamical variables, w^2 and $\|u_\perp\|^2$.

The energy input to the condensate from layers I is

$$\mathcal{I} = \int_{-k_f}^{-2\pi/L_x} \int_{\frac{2\pi}{L_z}}^{p_z^1} \frac{\epsilon_{p_x, p_z}}{2} dp_z dp_x = \frac{2\epsilon}{\pi} \int_{\frac{2\pi}{L_x}}^{k_f} dp_x \frac{1}{2k_f} \left[\arctan\left(\frac{p_z}{\sqrt{k_f^2 - p_x^2 - p_z^2}}\right) \right]_{\frac{2\pi}{L_z}}^{\frac{Sk_f}{4}} \\ \approx \frac{2\epsilon}{\pi} \int_{\frac{2\pi}{L_x}}^{k_f} dp_x \left(\frac{S}{8} - \frac{l_f}{2L_z} \right) \frac{1}{\sqrt{k_f^2 - p_x^2}} = \frac{2\epsilon}{\pi} \left(\frac{S}{8} - \frac{l_f}{2L_z} \right) \left[\arctan\left(\frac{p_x}{\sqrt{k_f^2 - p_x^2}}\right) \right]_0^{k_f} = \epsilon \left(\frac{S}{8} - \frac{l_f}{2L_z} \right), \quad (\text{E45})$$

where we have put the IR cutoff in p_x to zero in the last step, since the integral converges for small p_x . Note that 2D modes $p_z = 0$ are excluded, and that this contribution vanishes when $S/8 < \frac{l_f}{2L_z}$

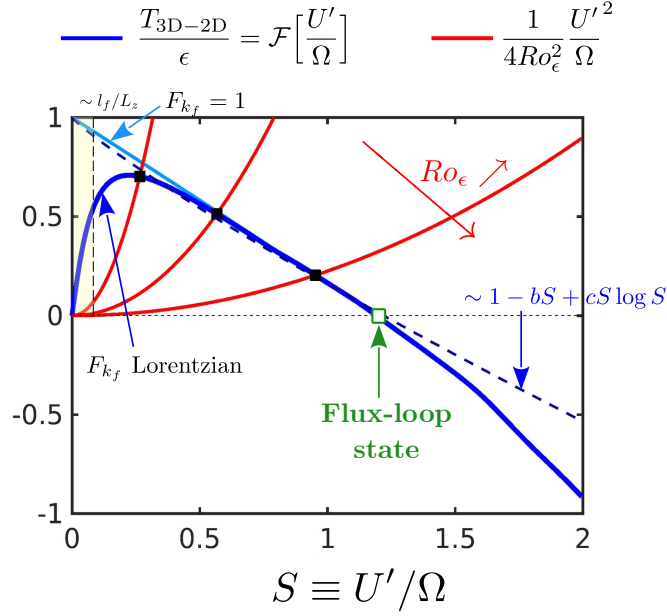


FIG. 7: Total energy transfer from the 3D waves to the 2D condensate as a function of $S \equiv U'/\Omega$. Integration is carried out without homochiral-wave filter F_{k_f} (light blue), and with a Lorentzian filter (E63) (blue), both without cutoff ($K \rightarrow \infty$). Dashed line: leading order behavior (E27). Red line: mean-flow dissipation $\nu U'^2 = \frac{S^2}{4Ro_\epsilon^2}$ for various values of Ro_ϵ . The solution to the mean-wave system is found at the intersection between the blue and the red line (black squares). The flux-loop state $T_{3D-2D} = 0$, obtained when $Ro_\epsilon \rightarrow \infty$, is marked as a green square. The yellow region $S < l_f/L_z$ indicates the range where interactions are mostly homochiral.

To obtain an estimate of the production of kinetic energy from Layers I (denoted by \mathcal{D}), for which $0 < p_y^* < p_y^f$, we can consider two limiting behaviors in Eq. (E35): $p_0 \ll p_y^*$ and $p_y^* \ll p_0$. These two limiting behaviors, which control the values of the arctan functions in (E35), correspond to different geometrical conditions on the value of p_z/p_x . Indeed, $p_0 \ll p_y^* \Leftrightarrow p_z^2 \left(\left(\frac{4}{S} \right)^2 - 2 \right) 2p_x^2$, which can be approximated as $p_z^2 > 2p_x^2 \left(\frac{S}{4} \right)^2$. Therefore, cases $p_0 \ll p_y^*$ and $p_y^* \ll p_0$ correspond to different values of the ratio $\frac{p_z^2}{2p_x^2} \left(\frac{4}{S} \right)^2$. We now split the integral of the term in $\frac{p_z^2}{p_x^2}$ in (E35), hereby denoted by \mathcal{D}_{p_x, p_z} , as:

$$\mathcal{D} \equiv \int \mathcal{D}_{p_x, p_z} \simeq \int_{\frac{2\pi}{L_x}}^{k_f} \int_{\frac{2\pi}{L_z}}^{\sqrt{2} \frac{p_x S}{4}} \mathcal{D}_{p_x, p_z} + \int_{\frac{2\pi}{L_x}}^{k_f} \int_{\sqrt{2} \frac{p_x S}{4}}^{\frac{k_f S}{4}} \mathcal{D}_{p_x, p_z} \quad (\text{E46})$$

Each integral is denoted, respectively, as $\int_1 \mathcal{D}_{p_x, p_z}$ and $\int_2 \mathcal{D}_{p_x, p_z}$.

If $p_0 \ll p_y^* \Leftrightarrow p_z > \sqrt{2} p_x \left(\frac{S}{4} \right)$, then $p_0 \ll p_y^f$ (as $p_y^* < p_y^f$), and therefore $p_y^f \simeq k_f$. Similarly, $p_0 \ll p_y^* \Rightarrow p_y^* \sim p^*$ then the arctan terms can be estimated like in Layer II, and

$$\mathcal{D}_{p_x, p_z} \simeq -\frac{\epsilon_{p_x, p_z}}{2} \frac{p_z^2}{p_x^2} \frac{k_f^2}{p_0^2} \left(\left(\frac{p_0}{p^*} \right)^2 + \left(\frac{\pi}{2} - \frac{p_0}{p_y^f} - \frac{\pi}{2} + \frac{p_0}{p_y^*} \right)^2 \right) \quad (\text{E47})$$

$$= -\frac{\epsilon_{p_x, p_z}}{U'} \frac{p_z^2}{p_x^2} k_f^2 \left(\left(\frac{S}{4p_z} \right)^2 + \left(\frac{S}{4p_z} - \frac{1}{k_f} \right)^2 \right) \quad (\text{E48})$$

$$= -\frac{\epsilon_{p_x, p_z}}{2} \frac{k_f^2}{p_x^2} \left(\left(\frac{S}{4} \right)^2 + \left(\frac{S}{4} - \frac{p_z}{k_f} \right)^2 \right) \quad (\text{E49})$$

Note that here we do not make any assumption on p_y^*/p_y^f . Upon integration in this geometrical sector, we obtain:

$$\int_2 \mathcal{D}_{p_x, p_z} = -\frac{2\epsilon}{\pi} \int_{\frac{2\pi}{L_x}}^{k_f} dp_x \int_{\frac{\sqrt{2} p_x S}{4}}^{k_f S} dp_z \frac{1}{2} \frac{1}{p_x^2} \left(\left(\frac{S}{4} \right)^2 + \left(\frac{S}{4} - \frac{p_z}{k_f} \right)^2 \right) \quad (\text{E50})$$

$$= -\frac{\epsilon}{\pi} \int_{\frac{2\pi}{L_x}}^{k_f} dp_x \frac{1}{p_x^2} \left[\left(\frac{S}{4} \right)^2 \left(\frac{k_f S}{4} - \frac{\sqrt{2} p_x S}{4} \right) - \frac{k_f}{3} \left[\left(\frac{S}{4} - \frac{p_z}{k_f} \right)^3 \right]_{\frac{\sqrt{2} p_x S}{4}}^{k_f S} \right] \quad (\text{E51})$$

$$= -\frac{\epsilon}{\pi} \left[\left(\frac{S}{4} \right)^3 \left(\frac{k_f L_x}{2\pi} - 1 \right) - \sqrt{2} \frac{S}{4} \log \left(\frac{k_f L_x}{2\pi} \right) \right] + \frac{k_f}{3} \int_{\frac{2\pi}{L_x}}^{k_f} \frac{1}{p_x^2} \left(\frac{S}{4} - \sqrt{2} \frac{p_x S}{k_f} \right)^3 \quad (\text{E52})$$

$$= -\frac{\epsilon}{\pi} \left[\left(\frac{S}{4} \right)^3 \left(\frac{k_f L_x}{2\pi} - 1 \right) - \sqrt{2} \frac{S}{4} \log \left(\frac{k_f L_x}{2\pi} \right) \right] + \frac{k_f}{3} \left[-\frac{L_x}{2\pi} \left(\frac{S}{4} \right)^3 - 3\sqrt{2} \left(\frac{S}{4} \right)^3 \log \left(\frac{k_f}{k_x} \right) \right] \quad (\text{E53})$$

$$\simeq -\frac{\epsilon}{\pi} \frac{2}{3} \frac{L_x k_f}{2\pi} \left(\frac{S}{4} \right)^3 + O \left(\left(\frac{S}{4} \right)^3 \log \left(\frac{L_x k_f}{2\pi} \right) \right) \quad (\text{E54})$$

Now, if $p_y^* \ll p_0$, the configuration is exactly that in layers Ia (where $p_y^* = 0$): the integrand \mathcal{D}_{p_x, p_z} is now independent of S , as all the p_z -layers are fully unaffected by rotation. It is convenient to approximate that $p_0 \ll p_y^f$ hence $p_y^f \sim k_f$ and $\epsilon_{p_x, p_z} \simeq \frac{\epsilon}{2\pi k_f^2 V}$. The case $p_y^f \rightarrow k_f$ gives an upper bound of the integrand as, $\arctan(p_y^f/p_0) < \pi/2$:

$$\mathcal{D}_{p_x, p_z} > -\frac{\epsilon_{p_x, p_z}}{2} \frac{p_z^2 k_f^2}{p_x^2 p_0^2} 2 \left(\frac{\pi}{2} \right)^2, \quad (\text{E55})$$

with in the . Integration of this term gives:

$$\int_1 \mathcal{D}_{p_x, p_z} = -\frac{2}{\pi} \int_{\frac{2\pi}{L_x}}^{k_f} dp_x \int_{\frac{2\pi}{L_z}}^{\sqrt{2} \frac{p_x S}{4}} dp_z \frac{\epsilon}{k_f^2} \frac{p_z^2}{p_x^2} \frac{k_f^2}{p_x^2 + p_z^2} \left(\frac{\pi}{2} \right)^2 \quad (\text{E56})$$

$$\simeq -\frac{2\epsilon}{\pi} \frac{\pi^2}{4} \int_{\frac{2\pi}{L_x}}^{k_f} dp_x \frac{1}{p_x^2} \left[p_z - p_x \arctan \left(\frac{p_z}{p_x} \right) \right]_{2\pi/L_z}^{\sqrt{2} S p_x / 4} \quad (\text{E57})$$

$$= -\frac{2\epsilon}{\pi} \frac{\pi^2}{4} \int_{\frac{2\pi}{L_x}}^{k_f} dp_x \left(\frac{S\sqrt{2}}{4p_x} - \frac{1}{p_x} \arctan \left(\sqrt{2} \frac{S}{4} \right) \right) - \left(\frac{r_z}{p_x} - \frac{1}{p_x} \arctan \left(\frac{r_z}{p_x} \right) \right) \quad (\text{E58})$$

$$= -\frac{2\epsilon}{\pi} \frac{\pi^2}{4} \log \left(\frac{k_f L_x}{2\pi} \right) \left(\frac{\sqrt{2} S}{4} - \arctan \left(\frac{\sqrt{2} S}{4} \right) \right) - O \left(\frac{L_x}{L_z} \right) \quad (\text{E59})$$

$$\simeq -\frac{2\epsilon}{\pi} \frac{\pi^2}{4} \log \left(\frac{k_f L_x}{2\pi} \right) \frac{1}{3} \left(\frac{S\sqrt{2}}{4} \right)^3 - O \left(\frac{L_x}{L_z} \right) \quad (\text{E60})$$

where in the last line we extend $S/4 \ll 1$ to $\sqrt{2}S/4 \ll 1$. Surprisingly, this term does not dominate in L_x , because modes $p_x \rightarrow 0$ are more numerous in the integral $\int_2 \mathcal{D}_{p_x, p_z}$, yielding a $L_x k_f$ dependence in (E54). The term $-O(L_x/L_z)$, written as a shortcut, causes $\int_1 \mathcal{D}_{p_x, p_z}$ to vanish when $\frac{2\pi}{L_z} = \frac{2\pi}{L_x} \sqrt{2} \frac{S}{4}$, consistently with the bound of this integral.

All in all, the contribution from layers I is approximated as

$$T_{3\text{D}-2\text{D}}^{\text{I}} \simeq \epsilon \left(\frac{S}{8} - \frac{l_f}{2L_z} - \frac{2}{3\pi} \frac{L_x}{l_f} \left(\frac{S}{4} \right)^3 \right), \quad (\text{E61})$$

up to corrections of $O(L_x/L_z)$ that make the last term vanish at $\frac{S}{4} = \frac{l_f}{L_z}$, consistently with the bounds of the original integral. The contribution of the layers is strictly zero when $S/4 < l_f/L_z$.

We see from (E61) that when $S \rightarrow 0$ the first term dominates, but then the growth with S is compensated by the second term and the net transfer decreases. However, the negative contribution remains small compared to $L_x/l_f S$ (the dominant term in Layers II). If $L_x k_f \rightarrow \infty$, as the flux-loop solution from Layers II happens at $S \simeq 8/(k_f L_x)$ (for which $T_{3\text{D}-2\text{D}}^{\text{II}} \simeq 0$), the $S/8$ contribution in (E61) dominates at this value of S and contributes at $O(S/4)$ in $T_{3\text{D}-2\text{D}}$. However, for the choice of parameters corresponding to our DNS ($L_z/l_f = 5$), $S/4 > l_f/L_z$ only for $S > 4/5$,

which is when the $-L_x/l_f(\frac{S}{4})^3$ dominates. Therefore, contributions from Layers I remain small compared to Layers II in this case, and we entirely neglect them.

With the parameter choice $L_x = \pi$, $k_f = 10$ corresponding to our DNS, layers I are actually fully negligible because $S/4 < l_f/L_z = 1/5$ for most the values of S . However, for this parameter choice, the term in $O\left(\frac{S}{4}\frac{L_x}{l_f}\left(\frac{l_f}{L_z}\right)^{1/2}\right)$, written explicitly in (E42), is not negligible. With its inclusion, the total transfer of energy is

$$T_{3D-2D} \approx T_{3D-2D}^{\text{II}} = \epsilon' \left[1 + \frac{1}{\pi} \sqrt{\frac{l_f}{2L_z}} - \frac{S}{4} \left(\frac{19}{12} \frac{L_x}{\pi l_f} + \frac{1}{2} - \frac{1}{2} \log \frac{S}{4} - \frac{1}{2\pi} \frac{L_x}{l_f} \sqrt{\frac{l_f}{2L_z}} \right) \right] \quad (\text{E62})$$

with $\epsilon' = \epsilon / (1 + \frac{1}{\pi} \sqrt{\frac{l_f}{2L_z}})$ the energy injection rate corrected to include discretization errors.

The function (E62) is shown in Figure 7 as a dashed blue line. With this estimate of the energy transfer, we obtain a flux-loop state $T_{3D-2D} = 0$ at $S \simeq 1.2$. We will compare this leading-order estimate with a numerical summation of the discrete Reynolds transfer (E36) in §E 4.

4. Numerical integration without cutoff

We now integrate numerically the Reynolds stress in Eq. (E36) over a discrete set of wavenumbers $p_z = 2\pi m_z/L_z$ and $p_x = 2\pi m_x/L_x$, where $m_z, m_x \in \mathbb{Z}$. This amounts to making a semi-continuous approximation only along p_y , which is still treated as a continuous variable. Note that we use the value of ϵ_{p_x, p_z} corresponding to the same discrete forcing as in the DNS, such that $\sum_{p_y} \epsilon_{p_x, p_z} = \epsilon$. In this section, we let the wavenumber cutoff $K \rightarrow \infty$.

Figure 7 shows the total energy transfer $T_{3D-2D}[S]$ in (E36), without homochiral-wave filter ($F_{k_f} = 1$, light blue), resulting from summing over discrete p_x, p_z and with the parameters corresponding to our DNS ($L_x/l_f = L_z/l_f = 5$). The asymptotic scaling (E27) is shown as a blue dashed line in Fig. 7. It reproduces the dominant behavior of the numerical integration of $T_{3D-2D}(S)$ (light blue line). This validates our leading-order expansion, and the fact that layers I can be fully neglected with our parameter choice. We have also verified that (E27) was realized with larger values of L_x/l_f and L_z/l_f , which we do not show here.

We now consider a filter F_{k_f} for the homochiral waves, and show the corresponding transfer $T_{3D-2D}(S)$ in Fig. 7 as a solid blue line. We chose a Lorentzian form for the homochiral-wave filter,

$$F_{k_f} = \frac{1}{1 + \left(\frac{1}{S} \frac{4\pi p_z \sqrt{k_f^2 - p_x^2 - p_z^2}}{L_y k_f^3} \right)^2}. \quad (\text{E63})$$

When including this filter, the theory captures the decoupling between the waves and the 2D flow occurring at large rotation ($S < l_f/L_y$), when resonances are more stringent. It leads to the decay of T_{3D-2D} when $S \rightarrow 0$. With such a smooth filter, the function T_{3D-2D} exhibits a smooth transition from the decoupling to the heterochiral regime, around $S \simeq 0.2$. A sharper filter for such resonant interactions, like the Heaviside function (B10), would result in a continuous but sharp transition between the two regimes.

Note, finally, that we have neglected 2D-2D interactions in this computation. With isotropic forcing, these should lead to an energy input $T_{2D-2D} \simeq l_f/(4L_z) \ll 1$ (see [30]), which is negligible for sufficiently large values of Ro_ϵ , but not too large. With this hypothesis, the energy injection rate ϵ corresponds to the energy input in 3D modes only. At low rotation, considering 2D-2D interactions goes beyond our QL theory, as they can disappear due to instabilities, which are not included in our framework.

Adding Layers I (Eq. (E45)), we obtain:

$$T_{3D-2D} \underset{K \gg k_f}{\approx} \epsilon \left[1 - \frac{l_f}{2L_z} - \frac{S}{4} \left(\frac{1}{\pi} \frac{19}{12} \frac{L_x}{\pi l_f} - \frac{1}{2} \log \frac{S}{4} \right) \right] \quad (\text{E64})$$

where the constant term, $\epsilon(1 - \frac{l_f}{2L_z}) \equiv \epsilon_{3D}$ is the fraction of energy injected in 3D modes $p_z \neq 0$ when forcing is isotropic.

5. Analytical solution without cutoff

From the leading-order expression of the energy transfer (E64), one can derive a simple solution to the quasi-linear system, valid in the regime where homochiral-wave have not decoupled ($S > l_f/L_y$) where $F_{k_f} = 1$.

using the mean-flow energy balance

$$\nu U'^2 = T_{3D-2D}, \quad (\text{E65})$$

which reads

$$\frac{1}{4Ro_\epsilon^2} S^2 = \frac{T_{3D-2D}}{\epsilon} [S], \quad (\text{E66})$$

with non-dimensional parameters $Ro_\epsilon = \frac{1}{2\Omega} \sqrt{\frac{\epsilon}{\nu}}$ and $S = U'/\Omega$. With the transfer T_{3D-2D} written explicitly in (E64), Equation (E66) is of the form

$$\frac{1}{4Ro_\epsilon^2} S^2 = 1 - bS + cS \log S \quad (\text{E67})$$

with

$$b = \frac{1}{4} \frac{\frac{19}{12} \frac{L_x}{\pi l_f} + \frac{1}{2} + \log 2 + \frac{1}{2\pi} \frac{L_x}{l_f} \sqrt{\frac{l_f}{2L_z}}}{1 + \frac{1}{\pi} \sqrt{\frac{l_f}{2L_z}}} \quad (\text{E68})$$

$$\approx \frac{1}{4} \left[\frac{19}{12} \frac{L_x}{\pi l_f} + \frac{1}{2} + \log 2 + \left(\frac{1}{2\pi} - \frac{1}{\pi} \left(\frac{3}{2} + \frac{1}{12} \right) \right) \frac{L_x}{l_f} \sqrt{\frac{l_f}{2L_z}} \right] + O\left(\sqrt{\frac{l_f}{L_z}}\right) + O\left(\frac{L_x}{l_f} \frac{l_f}{2L_z}\right) \quad (\text{E69})$$

and

$$c = \frac{1}{8} \frac{1}{1 + \frac{1}{\pi} \sqrt{\frac{l_f}{2L_z}}} \approx \frac{1}{8} \left(1 - \frac{1}{\pi} \sqrt{\frac{l_f}{2L_z}} \right), \quad (\text{E70})$$

including corrections in $O\left(\frac{L_x}{l_f} \sqrt{\frac{l_f}{L_z}}\right)$.

When expanding in $c/b \ll 1$, we first solve the leading-order solution with $c = 0$:

$$S^* = 2bRo_\epsilon^2 \left(-1 + \sqrt{1 + \frac{1}{b^2 Ro_\epsilon^2}} \right), \quad (\text{E71})$$

Solution to (E67) is written as $S = S^* + \delta S$, with δS solving at order c/b

$$\frac{2S^* \delta S}{4Ro_\epsilon^2} = -b\delta S + cS^* \log S^* \implies \delta S = c \frac{1}{b + \frac{S^*}{2Ro_\epsilon^2}} S^* \log S^* \quad (\text{E72})$$

Therefore we obtain

$$S = S^* \left[1 + c \frac{\log S^*}{b + \frac{S^*}{2Ro_\epsilon^2}} \right] \quad (\text{E73})$$

$$= 2bRo_\epsilon^2 \left(-1 + \sqrt{1 + \frac{1}{b^2 Ro_\epsilon^2}} \right) \left[1 + \frac{c}{b} \frac{\log \left(2bRo_\epsilon^2 \left(-1 + \sqrt{1 + \frac{1}{b^2 Ro_\epsilon^2}} \right) \right)}{\sqrt{1 + \frac{1}{b^2 Ro_\epsilon^2}}} \right] \quad (\text{E74})$$

This solution, correcting (E71), is shown in the main text Fig. 3(b) with $L_x/l_f = L_z/l_f = 5$, corresponding to our DNS choice. We show in Fig. 3(a) the corresponding energy transfer from the waves, obtained from (E66):

$$\frac{T_{3D-2D}[Ro_\epsilon]}{\epsilon} = \frac{S^2}{4Ro_\epsilon^2} = \frac{b}{2Ro_\epsilon^2} \left(-1 + \sqrt{1 + \frac{1}{b^2 Ro_\epsilon^2}} \right) \left[1 + \frac{c}{b} \frac{\log \left(2bRo_\epsilon^2 \left(-1 + \sqrt{1 + \frac{1}{b^2 Ro_\epsilon^2}} \right) \right)}{\sqrt{1 + \frac{1}{b^2 Ro_\epsilon^2}}} \right] \quad (\text{E75})$$

Appendix F: Cutting-off wave-wave and eddy-eddy interactions

1. Choice of cutoff

We now discuss the introduction of a wavenumber cutoff K , which, as we will see, provides a validity range for both quasi-linear hypothesis and wave kinetics. We first introduce various relevant timescales:

$$\tau_\Omega = \frac{p}{\Omega p_z}, \quad \text{twice the wave period} \quad (\text{F1})$$

$$\tau_{nl}^{\text{eddy}} = \epsilon^{-1/3} p^{-2/3}, \quad \text{the eddy-eddy interaction time} \quad (\text{F2})$$

$$\tau_{nl}^{\text{wave}} = \Omega^{1/2} \epsilon^{-1/2} p_z^{1/2} p_\perp^{-3/2}, \quad \text{the wave-wave interaction time} \quad (\text{F3})$$

The eddy turnover time τ_{nl}^{eddy} is determined from the Kolmogorov scaling, while the wave-wave interaction time scale τ_{nl}^{wave} is predicted from wave-turbulent theory [53].

These time scales lead to the definition of various p_z -dependent wavenumbers:

$$k_\Omega = \Omega^{3/5} \epsilon^{-1/5} p_z^{3/5}, \quad \text{the crossover from waves to eddies} \quad (\text{F4})$$

$$k_U^{\text{wave}} = (\Omega p_z)^{1/3} U'^{2/3} \epsilon^{-1/3}, \quad \text{the crossover from condensate- to wave-dominated interactions} \quad (\text{F5})$$

$$k_U^{\text{eddy}} = U'^{3/2} \epsilon^{-3/2}, \quad \text{the crossover from condensate- to eddy-dominated interactions.} \quad (\text{F6})$$

These various wavenumbers are explained in the following.

Wavenumber k_Ω in (F4) denotes the crossover wavenumber delimiting wave-like ($p < k_\Omega \iff \tau_\Omega < \tau_{nl}^{\text{eddy}}$) from eddy-like ($p > k_\Omega \iff \tau_{nl}^{\text{eddy}} < \tau_\Omega$) behaviors, called the Zeman wavenumber. Here we define by ‘‘waves’’ rotation-dominated modes, as opposed to ‘‘eddies’’.

Nonlinear interactions between fluctuation modes occur over a nonlinear time scale τ_{nl} , whose estimation depends on whether mode \mathbf{p} is wave-dominated ($p < k_\Omega$) or eddy-dominated ($p > k_\Omega$). When modes are wave-dominated, they interact with other waves over a slow nonlinear timescale τ_{nl}^{wave} in (F3), which is $\gg \tau_\Omega$. In contrast, when modes are eddy-dominated, they interact with each other over the Kolmogorov time scale τ_{nl}^{eddy} in (F2).

The quasi-linear assumption is valid when mean-fluctuation interactions dominate over nonlinear interactions within fluctuations, i.e when $1/U' < \tau_{nl}$. Depending on whether modes are eddy or wave-dominated, this leads to two definitions for the crossover wavenumber k_U , k_U^{wave} in (F5) and k_U^{eddy} in (F6), above which interactions with the mean flow are negligible.

Wave-dominated modes ($p < k_\Omega$), if $\tau_{nl}^{\text{wave}} < 1/U'$, are outside the QL framework. Therefore, modes above k_U^{wave} (F5) must be cutoff from the QL computation. Waves obeying the QL assumption, i.e such that $p < k_U^{\text{wave}}$, can lie either in Sector H or in Sector A, depending if τ_Ω is above or below $1/U'$. When rotation is sufficiently large, most modes behave as waves, and only the cutoff k_U^{wave} needs to be considered. This high-rotation case is illustrated in Fig. 8a.

Eddy-dominated modes ($p > k_\Omega$), which appear at low rotation, obey a different time-scale hierarchy, illustrated in Fig. 8b. When eddies ($\tau_{nl}^{\text{eddy}} < \tau_\Omega$) dominantly interact with the mean flow ($1/U' < \tau_{nl}^{\text{eddy}}$), they are such that $1/U' < \tau_\Omega$, hence, from condition (B13), they necessarily belong to the heterochiral Sector A. This is a consequence of the fact that eddies *cannot be homochiral-only when interacting with the condensate*, as expected from them being unaffected by rotation hence not subject to resonant constraints. As a consequence, the homochiral Sector H only concerns wave-like modes and not eddies and must cutoff at k_Ω . In contrast, Sector A can sustain both waves and eddies: the former being cutoff at k_U^{wave} , the latter at k_U^{eddy} . Modes in Sector A are therefore necessarily cutoff at $\min(k_U^{\text{eddy}}, k_U^{\text{wt}})$ to obey the QL condition.

All in all, we define the cutoff wavenumber as

$$K(p_z, \Omega, U') = \begin{cases} k_U^{\text{wave}} & \text{if } k_U^{\text{wave}} < k_\Omega \text{ and } k_U^{\text{wave}} < k_U^{\text{eddy}} \\ \begin{cases} k_\Omega & \text{if } \tau_\Omega < \frac{1}{U'} \quad (\text{Sector H}) \\ \min(k_U^{\text{eddy}}, k_U^{\text{wave}}) & \text{if } \tau_\Omega \geq \frac{1}{U'} \quad (\text{Sector A}) \end{cases} \end{cases} \quad (\text{F7})$$

to cover both wave-dominated and eddy-dominated cases.

The dominant effect of this cutoff appears at low rotation, where both k_Ω and $k_U^{\text{eddy}} \ll k_U^{\text{waves}}$. Here, Sector H is cutoff at k_Ω and Sector A at k_U^{eddy} . The presence of a cutoff in Sector H at k_Ω strongly affects the energy input to the condensate from Sector H. As $Ro \rightarrow 0.5$, $k_\Omega(p_z = k_f) \rightarrow k_f$, and the contribution from sector H progressively vanishes, as illustrated in Fig. 8(c). This causes the condensate to vanish at $Ro \simeq 0.5$ to a state of pure eddy turbulence.

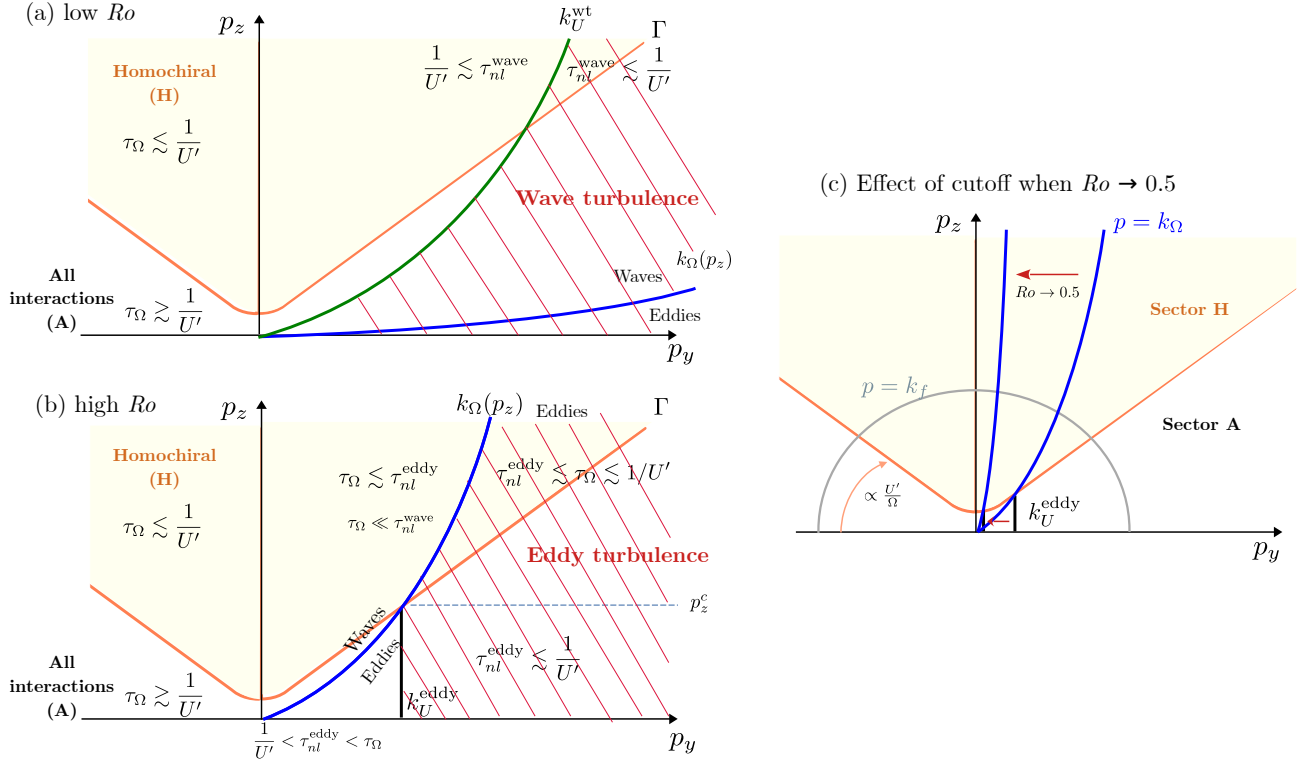


FIG. 8: Hierarchy of time scales and choice of cutoffs at (a) high and (b) low rotation. Sector H ($\tau_\Omega < 1/U'$) is colored in yellow, and Sector A ($\tau_\Omega \geq 1/U'$) is in white. Here we fix the value of U'/Ω , hence the boundary between sectors H and A. The Zeman scale k_Ω (F4) (blue curve) delimits wave-like from eddy-like behaviors. Waves dominate at low Ro (a), and wave-wave interactions dominate $p > k_U^{\text{wave}}(p_z)$ (F5) (green line). Eddies dominate at large Ro (b), and eddy-eddy interactions dominate for $p > k_U^{\text{eddy}}$ (F6) in sector A and $p > k_\Omega(p_z)$ in sector H (blue lines). Modes above these cutoffs do not interact with the condensate and are not considered in the QL theory. Note that $k_U^{\text{wave}} \ll k_U^{\text{eddy}}$ in (a), while $k_U^{\text{eddy}} \ll k_U^{\text{wave}}$ in (b). (c) Evolution of cutoff $K(p_z)$ at low rotation, when $Ro \rightarrow 0.5$. At fixed $S = U'/\Omega$, fewer waves in Sector H are excited as $Ro \rightarrow 0.5$. When $Ro = 0.5$ and $k_\Omega(p_z = k_f) = k_f$, no homochiral waves are excited and the energy input to the condensate vanishes.

2. Numerical integration of the Reynolds stress with cutoff

We now describe how to solve the quasi-linear system numerically, and how its solution depends on the parameters of the system, in particular cutoff K . The condensate amplitude U'/Ω solves in steady state the mean-flow energy balance

$$\frac{1}{4Ro_\epsilon^2} \frac{U'^2}{\Omega^2} = \frac{T_{3D-2D}}{\epsilon} \left[\frac{U'}{\Omega}, Ro \right], \quad (\text{F8})$$

where $T_{2D} \left[\frac{U'}{\Omega}, Ro \right]$ is given explicitly in Eq. (E36) via our integration of the Reynolds stress. The additional Ro dependence arises through cutoff K defined in (F7).

In order to compare the QL theory with our DNS of rotating 3DNSE, we numerically integrate the Reynolds stress in Eq. (E36) over a discrete set of wavenumbers $p_z = 2\pi m_z/L_z$ and $p_x = 2\pi m_x/L_x$, where $m_z, m_x \in \mathbb{Z}$. This amounts to making a semi-continuous approximation only along p_y , which is still treated as a continuous variable. Note that we use the value of ϵ_{p_x, p_z} corresponding to the same discrete forcing as in the DNS, such that $\sum_{p_y} \epsilon_{p_x, p_z} = \epsilon$,

Once $T_{3D-2D} \left[\frac{U'}{\Omega}, Ro \right]$ is computed from (E36), we solve (F8) by finding the intersection between $S^2/(4Ro_\epsilon^2)$ and $T_{3D-2D}/\epsilon[S, Ro]$ (where $S = U'/\Omega$) for all values of Ro and Re , see Fig. 7. The intersection is found by a numerical root-finding procedure. This results in a function

$$\frac{U'}{\Omega} = \mathcal{F}[Ro_\epsilon, Ro], \quad (\text{F9})$$

which we show in Fig. 9(a) as a function of Ro , and Fig. 9(b) as a function of $Ro_\epsilon = Ro \times Re^{1/2}$. The solution is shown for various values of Re .

When integrating numerically the Reynolds stress, we consider the Lorentzian filter for the homochiral-wave resonances (E63). It yields a smooth transition between the homochiral regime and the mixed-interaction regime around $Ro_\epsilon \simeq 0.1$ (see Fig. 9). This near-resonant treatment is more accurate at intermediate Ro_ϵ , as it captures the contribution of small near-resonances. However, it fails in the limit $Ro_\epsilon \rightarrow 0$, as explained in [30].

We furthermore introduce a parameter $\tilde{\omega}$ setting the time-scale ratio over which heterochiral interactions occur: we use the near-resonant condition

$$\omega_p^+ + \omega_q^- < \tilde{\omega}U' \quad (\text{F10})$$

in place of (B13). This is equivalent to changing S to $\tilde{\omega}S$ in (E36). Parameter $\tilde{\omega}$, which must be ~ 1 , provides an adaptable broadening of the resonant condition. It corresponds to approximating the oscillating factor $\Delta(t)^{s,-s}$ (B9) with a parametrized Heaviside function $\Theta(1 - |\omega_{pq}^+|/(\tilde{\omega}U'))$. In the results established so far, and in the solution shown in Fig. 4 of the main text, $\tilde{\omega}$ is set to 1. In general, $\tilde{\omega}$ can be used as a tunable parameter of the numerical integration which can better fit the DNS data points. In Figs. 9(a,b), we use $\tilde{\omega} = 1.2$. Solutions with $\tilde{\omega} = 1$ and $\tilde{\omega} = 1.2$ are compared in Fig. 9(c) and (d), respectively.

Due to the flux-loop behavior at low rotation, the high- Re solution of U'/Ω in (F9) changes its functional behavior as Ro is increased. It deviates from a single dependence on $Ro_\epsilon \equiv RoRe^{1/2}$ at low Ro to a single dependence in Ro at high Ro . This is visible in Fig 9(a). Cutoff $K(p_z)$ in (F7) controls the number of modes interacting with the condensate, hence its energy input, controlled by the value of Ro . Without cutoff, U'/Ω tends to a Ro -independent value when $Ro_\epsilon \rightarrow \infty$, hence $U' \propto Ro^{-1}$. With cutoff, whose effect is particularly important at high Ro where $K(p_z) \simeq k_\Omega(p_z)$, the number of waves shrinks when $Ro \rightarrow 0.5$, as $k_\Omega(p_z = k_f) \simeq k_f$. This wave shortage causes the condensate amplitude U'/Ω to decay to 0 at $Ro \simeq 0.5$, as seen in Figs. 9(a).

The introduction of a cutoff K has direct consequences on the dependence of U'/Ω on Re . This is illustrated in Figs. 9(b-d), where the integration is shown without cutoff ($K \rightarrow \infty$, dashed lines) and with cutoff (finite K , colors). Without cutoff, U'/Ω only depends on Ro_ϵ and saturates as $Ro_\epsilon \rightarrow \infty$. With cutoff, U'/Ω decays at a finite $Ro_\epsilon^* \simeq 0.5/Re^{1/2}$. When Re is increased, the decay of U'/Ω at Ro_ϵ^* is shifted to even larger Ro_ϵ^* when $Re \rightarrow \infty$. Therefore, the solution at large Ro_ϵ never collapses to the single Ro_ϵ -dependence obtained in the non-cutoff case, where $U'/\Omega \xrightarrow{Ro_\epsilon \rightarrow \infty} \text{cste}$.

Furthermore, our introduction of a cutoff generates an overshoot of the solution as Re is increased, compared to the non-cutoff solution: as seen from Fig. 7(c), at fixed Ro_ϵ , U'/Ω first increases and then decreases with Re , hence the value at finite Re overshoots that at $Re \rightarrow \infty$. This behavior is due to a non-monotonous dependence of the energy transfer T_{3D-2D} (E36) on cutoff wavenumber $K(p_z)$ at fixed $\frac{U'}{\Omega}$, which is inherent to our computation. This can be understood when only considering a cutoff at k_Ω in Sector H, and disregarding cutoff k_U : when increasing k_Ω , the number of modes in Sector H first increases and so does T_{3D-2D} , until all Sector H contributes. However, increasing k_Ω also results in a larger value of p_z^c , hence in a larger contribution of the heterochiral sector A. This causes T_{3D-2D} to decrease with K as more and more a Then, cutoff occurs only in Sector A, and T_{3D-2D} decreases with K as more and more modes take energy away from the mean flow. This behavior is independent of the choice of the function $K(p_z)$.

The QL computation involving cutoff K is compared to the DNS data points in Figs. 9(c-d). The agreement is quantitatively excellent up to $Ro_\epsilon \simeq 0.5$. At large Ro_ϵ , the behavior is sensitive to the cutoff and U'/Ω decays due to a wave shortage, and reaches zero at $Ro \simeq 0.5$. Our QL result qualitatively reproduces the decay of U'/Ω at fixed Re , and the transition to strong turbulence seen in the DNS. In addition, we obtain a close quantitative agreement at $Re = 23$ and 46 when using parameter $\tilde{\omega} = 1.2$. (Note that we obtain also a good quantitative agreement with the non-cutoff case $\tilde{\omega} = 1$ below $Ro_\epsilon = 1$).

However, the results of the QL theory for $Re > 46$ start to deviate from the DNS data points above $Ro_\epsilon \simeq 0.5$. This is largely due to the overshoot described above, which yields a non-monotonous trend in Re and fixed Ro_ϵ . This behavior is not observed in the DNS. Note that it might be possible to reduce this overshoot when including viscosity in the QL framework.

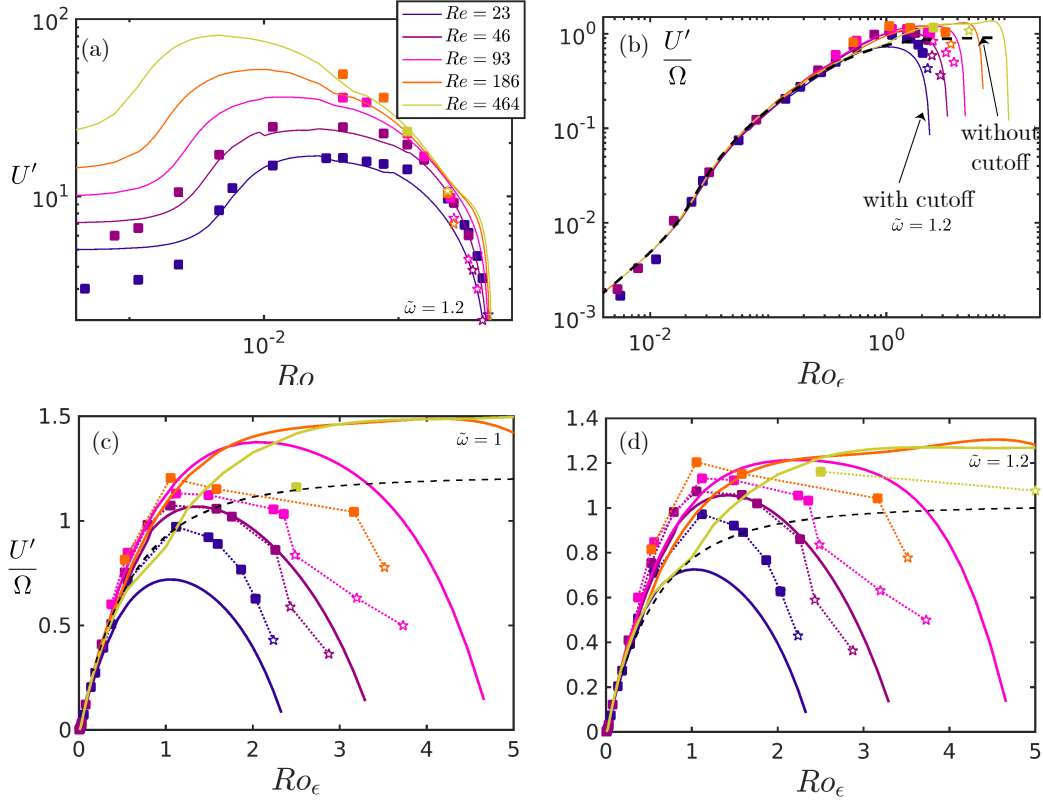


FIG. 9: Numerical solution of the quasi-linear system (F8), with (solid lines) and without (dashed lines) cutoff K (F7). (a) U' as a function of Ro , showing the collapse on Ro at large Ro . (b) U'/Ω as a function of $Ro_\epsilon = RoRe^{1/2}$, showing the collapse on Ro_ϵ at low Ro_ϵ . All QL results in (a,b) are obtained with $\tilde{\omega} = 1.2$. (c,d) Effect of $\tilde{\omega}$ on solution U'/Ω , visualized in linear scale: (c) $\tilde{\omega} = 1$, (d) $\tilde{\omega} = 1.2$, which better fits the DNS result.

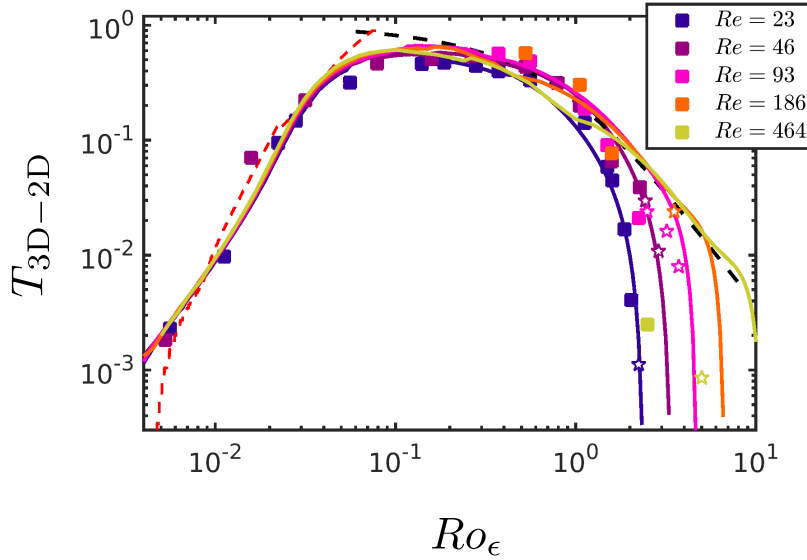


FIG. 10: Energy transfer to the 2D flow, T_{3D-2D}/ϵ , as a function of Ro_ϵ . Theoretical lines show the numerical QL solution with $\tilde{\omega} = 1.2$. The black dashed line shows the analytical solution without cutoff, Eq. (E75).